

ssROC: Semi-Supervised ROC Analysis for Reliable and Streamlined Evaluation of Phenotyping Algorithms

Jianhui Gao^{†1}, Clara-Lea Bonzel^{†2}, Chuan Hong³, Paul Varghese⁴, Karim Zakir¹, and Jessica Gronsbell^{1,5,6}

¹*Department of Statistical Sciences, University of Toronto, Toronto, ON, Canada*

²*Department of Biomedical Informatics, Harvard Medical School, Boston, MA, USA*

³*Department of Biostatistics and Bioinformatics, Duke University, Durham, NC, USA*

⁴*Verily Life Sciences, Cambridge, MA, USA*

⁵*Department of Family and Community Medicine, University of Toronto, Toronto, ON, Canada*

⁶*Department of Computer Science, University of Toronto, Toronto, ON, Canada*

Correspondence to:

Jessica Gronsbell

Postal address: 700 University Ave, Toronto, ON, Canada, M5G 1Z5

Email: j.gronsbell@utoronto.ca.

Telephone number: 416-978-3452

Keywords: Electronic Health Records; Phenotyping; Semi-supervised; ROC Analysis

Word count: 3980/4000

ABSTRACT

Objective: High-throughput phenotyping will accelerate the use of electronic health records (EHRs) for translational research. A critical roadblock is the extensive medical supervision required for phenotyping algorithm (PA) estimation and evaluation. To address this challenge, numerous weakly-supervised learning methods have been proposed to estimate PAs. However, there is a paucity of methods for reliably evaluating the predictive performance of PAs when a very small proportion of the data is labeled. To fill this gap, we introduce a semi-supervised approach (ssROC) for estimation of the receiver operating characteristic (ROC) parameters of PAs (e.g., sensitivity, specificity).

Materials and methods: ssROC uses a small labeled dataset to nonparametrically impute missing labels. The imputations are then used for ROC parameter estimation to yield more precise estimates of PA performance relative to classical supervised ROC analysis (supROC) using only labeled data. We evaluated ssROC through in-depth simulation studies and an extensive evaluation of eight PAs from Mass General Brigham.

Results: In both simulated and real data, ssROC produced ROC parameter estimates with significantly lower variance than supROC for a given amount of labeled data. For the eight PAs, our results illustrate that ssROC achieves similar precision to supROC, but with approximately 60% of the amount of labeled data on average.

Discussion: ssROC enables precise evaluation of PA performance to increase trust in observational health research without demanding large volumes of labeled data. ssROC is also easily implementable in open-source R software.

Conclusion: When used in conjunction with weakly-supervised PAs, ssROC facilitates the reliable and streamlined phenotyping necessary for EHR-based research.

BACKGROUND AND SIGNIFICANCE

Electronic Health Records (EHRs) are a vital source of data for clinical and translational research [1]. Vast amounts of patient data are being tapped for real-time studies of infectious diseases, development of clinical decision support tools, and genetic studies at unprecedented scale [2–10]. This myriad of opportunities rests on the ability to accurately and rapidly extract a wide variety of patient phenotypes (e.g., diseases) to both identify and characterize populations of interest. However, precise and readily available phenotype information is rarely available in patient records and presents a major barrier to EHR-based research [11, 12].

In practice, phenotypes are extracted from patient records with either rule-based or machine learning (ML)-based phenotyping algorithms (PAs) derived from codified and natural language processing (NLP)-derived features [13, 14]. While PAs can characterize clinical conditions with high accuracy, they traditionally require a substantial amount of medical supervision that limits the automated power of EHR-based studies [15]. Several research networks have spent considerable effort developing PAs over the last decade, including i2b2 (Informatics for Integrating Biology & the Bedside), the eMERGE (Electronic Medical Records and Genomics) Network, and the OHDSI (Observational Health Data Sciences and Informatics) program that released the APHRODITE (Automated PHenotype Routine for Observational Definition, Identification, Training, and Evaluation) framework [16].

Typically, PA development consists of two key steps: (i) algorithm estimation and (ii) algorithm evaluation. Algorithm estimation determines the appropriate aggregation of

features extracted from patient records to determine phenotype status. For a rule-based approach, medical and informatics experts assemble a comprehensive set of features and corresponding logic to assign patient phenotypes [12, 13]. As this manual assembly can be highly laborious, significant effort has been made to automate the algorithm estimation step with ML. Numerous studies have demonstrated success with PAs derived from standard supervised learning methods such as penalized logistic regression, random forest, and deep neural networks [17–24]. The scalability of a supervised approach, however, is limited by the substantial number of gold-standard labels required for model training. Gold-standard labels, which require time-consuming manual medical chart review, are infeasible to obtain for a large volume of records [25, 26].

In response, semi-supervised and weakly-supervised methods for PA estimation that substantially decrease or eliminate the need for gold-standard labeled data have been proposed. Among semi-supervised methods, self-learning and surrogate-assisted semi-supervised learning are common [27–29]. For example, [15] introduced PheCAP, a common pipeline for semi-supervised learning that utilizes silver-standard labels for feature selection prior to supervised model training to decrease the labeling demand. Unlike gold-standard labels, silver-standard labels can be automatically extracted from patient records (e.g., ICD codes or free-text mentions of the disease) and serve as proxies for the gold-standard label [30, 31]. PheCAP was based on the pioneering work of [32] and [33], which introduced weakly-supervised PAs trained entirely on silver-standard labels. These methods completely eliminate the need for medical chart review for algorithm estimation and are the basis of the APHRODITE framework. Moreover, this work prompted numerous developments in weakly-supervised PAs, including methods based on non-negative matrix/tensor factorization, parametric mixture modeling, and neural network-based em-

bedding learning, which are quickly becoming the new standard in the PA literature [14].

In contrast to the success in automating PA estimation, there has been little focus on the algorithm evaluation step. Algorithm evaluation assesses the predictive performance of a PA, typically through the estimation of the receiver operating characteristic (ROC) parameters such as sensitivity and specificity. At a high-level, the ROC parameters measure how well a PA discriminates between phenotype cases and controls relative to the gold-standard obtained from chart review. As phenotypes are the foundation of EHR-based studies, it is critical to reliably evaluate the ROC parameters to provide researchers with a sense of trust in using a PA [34–36]. However, complete PA evaluation is performed far too infrequently due to the burden of chart review [14, 25, 37].

To address this challenge, [38] proposed the first semi-supervised method for ROC parameter estimation. This method assumes that the predictive model is derived from a penalized logistic regression model and was only validated on 2 PAs with relatively large labeled data sets (455 and 500 labels). [25] later introduced PheValuator, and its recent successor PheValuator 2.0, to efficiently evaluate rule-based algorithms using “probabilistic gold-standard” labels generated from diagnostic predictive models rather than chart review [37]. Although the authors provided a comprehensive evaluation for numerous rule-based PAs, PheValuator can lead to biased ROC analysis, and hence a distorted understanding of the performance of a PA, when the diagnostic predictive model is not well-calibrated [39–41]. PheValuator is also only applicable for the evaluation of rule-based PAs.

To fill this gap in the PA literature, we introduce the semi-supervised approach of [38]

to precisely estimate the ROC parameters of PAs, which we call “ssROC”. The key difference between ssROC and classical ROC analysis (supROC) using only labeled data is that ssROC imputes missing gold-standard labels in order to leverage large volumes of unlabeled data (i.e., records without gold-standard labels). By doing so, ssROC yields less variable estimates than supROC to enable reliable PA evaluation with fewer gold-standard labels and hence significantly less chart review. Moreover, ssROC imputes the missing labels with a nonparametric recalibration of the predictions from the PA to ensure that the resulting estimates of the ROC parameters are unbiased when the PA is not well-calibrated.

OBJECTIVE

The primary objectives of this work are to:

1. Extend the proposal of [38] to a wider class of weakly-supervised PAs that are commonly used in the PA literature, including a theoretical analysis and development of a statistical inference procedure demonstrating good finite-sample properties.
2. Provide an in-depth real data analysis of PAs for eight phenotypes from Mass General Brigham (MGB) together with extensive simulation studies to illustrate the practical utility of ssROC.
3. Release an implementation of ssROC in open-source R software to encourage the use of our method by the informatics community.

Through our real and simulated data analyses, we observe substantial gains in estimation precision from ssROC relative to supROC. In the analysis of the eight PAs from MGB, ssROC achieves similar precision to supROC, but with approximately 60% of the amount

of labeled data on average. Our results suggest that, when used together with weakly supervised PAs, ssROC can facilitate the reliable and streamlined PA development that is necessary for EHR-based research.

MATERIALS AND METHODS

Overview of ssROC

We focus on evaluating a classification rule derived from a PA with ROC analysis. ROC analysis assesses the agreement between the gold-standard label for a binary phenotype (e.g., disease case/control), Y , and a PA score, S , indicating a patient’s likelihood of having the underlying phenotype (e.g., the predicted probability of being a disease case). Y is typically obtained from chart review and S can be derived from various phenotyping methods. In this article, we primarily consider PAs derived from weakly-supervised learning methods due to their ability to automate PA estimation and increasing popularity in the informatics literature [14].

In classical supervised ROC analysis, it is assumed that the data is fully labeled and one has information on both Y and S for all subjects. However, in the phenotyping setting, Y is typically only available for a very small subset of patient records due to the laborious nature of medical chart review. This gives rise to the *semi-supervised setting* in which a small labeled dataset is accompanied by a much larger unlabeled dataset. To fully leverage all of the available data and facilitate more reliable (i.e., lower variance) evaluation of PAs, ssROC imputes the missing Y with a nonparametric recalibration of S , denoted as $\hat{m}(S)$, to make use of the unlabeled data. A schematic representation of ssROC is provided in Figure 1.

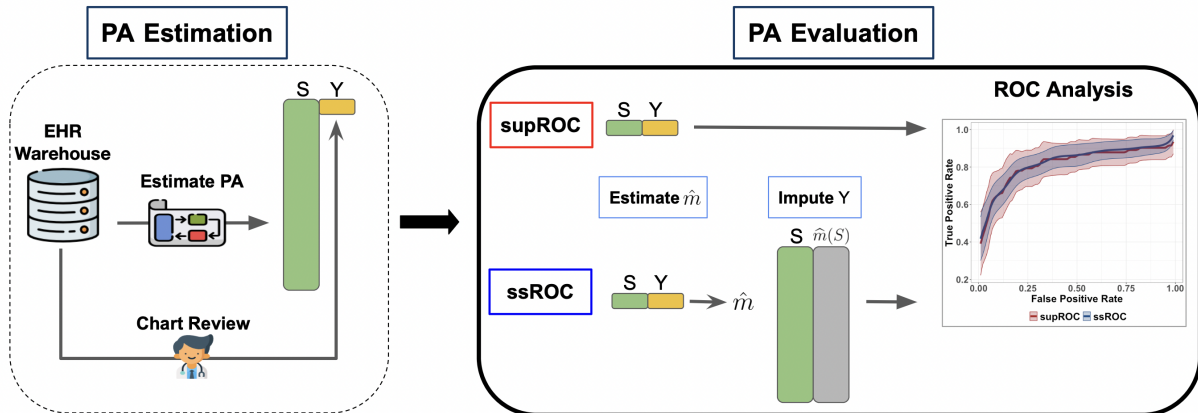


Figure 1: **Overview of PA estimation and evaluation.** The phenotyping algorithm (PA) is first estimated to obtain the scores (S). Patient charts from the electronic health record (EHR) warehouse are also reviewed to obtain the gold-standard label (Y) for PA evaluation. In classical supervised ROC analysis (supROC), only the labeled data from chart review is used to evaluate the PA’s performance. Semi-supervised ROC analysis (ssROC), uses the labeled data to impute the missing Y as $\hat{m}(S)$ so that the unlabeled data can be utilized for estimation to yield more precise estimates of the ROC parameters.

Data structure & notation

More concretely, the available data in the semi-supervised setting consists of a small labeled dataset with independently and identically distributed observations,

$$\mathcal{L} = \{(Y_i, S_i) \mid i = 1, \dots, n\}$$

and an independent unlabeled dataset

$$\mathcal{U} = \{S_i \mid i = n + 1, \dots, n + N\}.$$

Additionally, (i) \mathcal{U} is assumed to be much larger than \mathcal{L} so that $n \ll N$ and (ii) the observations in \mathcal{L} are randomly selected from the underlying pool of data. Throughout our discussion, we suppose that a higher value of S is more indicative of the phenotype.

An observation is deemed to have the phenotype if $S > c$, where c is the threshold used for phenotype classification.

ROC analysis

More formally, ROC analysis evaluates a PA based on the true positive rate (TPR), the false positive rate (FPR), the positive predictive value (PPV), and the negative predictive value (NPV). In the diagnostic testing literature, the TPR is referred to as sensitivity, while the FPR is 1 minus the specificity [42]. For a given classification threshold, one may evaluate the ROC parameters by enumerating the correct and incorrect classifications. This information can be summarized in a confusion matrix, as in Figure 2.

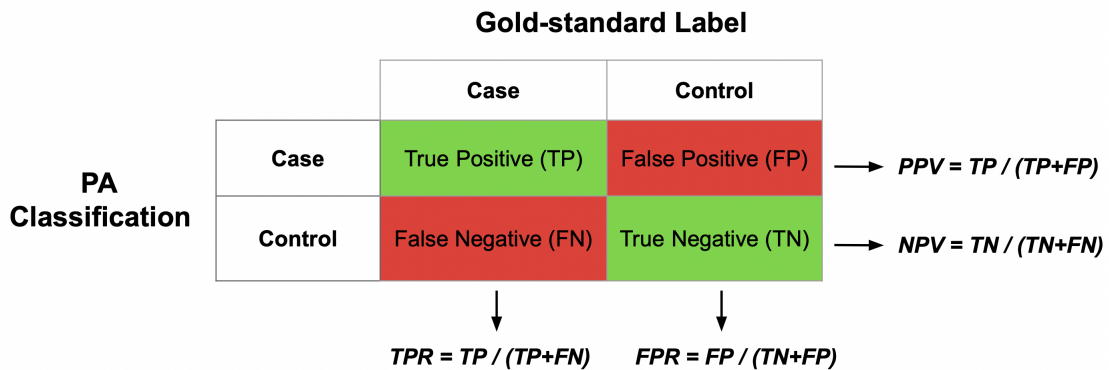


Figure 2: **Confusion matrix.** The algorithm score from the PA is used to determine phenotype case/control status based on the classification threshold. The ROC parameters can then be evaluated by enumerating the number of correct and incorrect classifications relative to the gold-standard label.

In practice, it is the task of the researcher to estimate an appropriate threshold for classification. This is commonly done by summarizing the trade-off between the TPR and

FPR, defined as

$$\text{TPR}(c) = P(S > c \mid Y = 1) \text{ and } \text{FPR}(c) = P(S > c \mid Y = 0).$$

The ROC curve, $\text{ROC}(u) = \text{TPR}[\text{FPR}^{-1}(u)]$, summarizes the TPR and FPR across all possible choices of the threshold. In the context of PAs, c is often chosen to achieve a low FPR, particularly when the prevalence of the phenotype is low [22]. An overall summary measure of the discriminative power of S in classifying Y is captured by the area under the ROC curve (AUC),

$$\text{AUC} = \int_0^1 \text{ROC}(u) du.$$

The AUC is equivalent to the probability that a phenotype case has a higher value of S than a phenotype control. For a given threshold, the predictive performance of the classification rule derived from the PA is assessed with the PPV and NPV, defined as

$$\text{PPV}(c) = P(Y = 1 \mid S > c), \quad \text{and} \quad \text{NPV}(c) = P(Y = 0 \mid S < c).$$

supROC: classical supervised ROC analysis

With only labeled data, one may obtain supervised estimators of the ROC parameters (supROC) based on their empirical counterparts. For example, the TPR and FPR can be estimated as

$$\widehat{\text{TPR}}_{sup}(c) = \frac{\sum_{i=1}^n Y_i I(S_i > c)}{\sum_{i=1}^n Y_i} \text{ and } \widehat{\text{FPR}}_{sup}(c) = \frac{\sum_{i=1}^n (1 - Y_i) I(S_i > c)}{\sum_{i=1}^n (1 - Y_i)}$$

for a given c . The PPV and NPV can be estimated analogously. A point along the ROC

curve is given by $\widehat{\text{ROC}}_{sup}(u_0) = \widehat{\text{TPR}}_{sup}(\hat{c}_{u_0}) = \widehat{\text{TPR}}_{sup} \left[\widehat{\text{FPR}}_{sup}^{-1}(u_0) \right]$ while the AUC may be obtained from standard numerical integration of the estimated ROC curve [43]. Variance estimates are obtained with a resampling-based procedure such as bootstrap or perturbation resampling [44, 45].

ssROC: semi-supervised ROC Analysis

Unlike its supervised counterpart that relies on only \mathcal{L} , ssROC utilizes both \mathcal{L} and \mathcal{U} to yield more precise estimates of the ROC parameters. To do so, ssROC consists of two steps of estimation (Figure 1). In the first step, the missing labels in \mathcal{U} are imputed with a nonparametric recalibration of the PA scores via local constant regression with \mathcal{L} . In contrast to using the PA scores directly for imputation, this step ensures that the ROC estimates are robust to potential bias from poor calibration of the PA [40]. Intuitively, this choice of imputation provides ssROC with the best guess of Y based on S for ROC analysis [40]. In the second step, ssROC uses the imputations and PA scores in \mathcal{U} to estimate the ROC parameters. This step produces estimates that have lower variance than supROC as \mathcal{U} is assumed to be much larger than \mathcal{L} . Practically, the purpose of ssROC is to enable a more reliable understanding of a PA’s performance by yielding less variable estimates relative to supROC without requiring more labeled data. Using the TPR for illustration, the ssROC method is detailed in Figure 3.

The conditions on the bandwidth in Step 1 ensure that $\hat{m}(\cdot)$ is undersmoothed to prevent bias in the estimated ROC parameter [46]. Additionally, the imputations obtained in Step 1 can be used in an analogous manner to compute the remaining ROC parameters. Similar to supROC analysis, we propose a perturbation resampling procedure for variance estimation and detail two commonly used confidence intervals (CIs) based on the

Overview of ssROC

Step 1. Estimate $m(s) = P(Y = 1 | S = s)$ with \mathcal{L} via local constant regression as

$$\hat{m}(s) = \frac{\sum_{i=1}^n K_h(S_i - s) Y_i}{\sum_{i=1}^n K_h(S_i - s)}$$

where $K_h(u) = h^{-1}K(u/h)$ is a given smooth, symmetric kernel function, h is a bandwidth controlling the smoothing, and $nh^2 \rightarrow \infty$ and $nh^4 \rightarrow 0$ as $n \rightarrow \infty$.

Step 2. Impute the missing labels in \mathcal{U} with $\hat{m}(\cdot)$ and evaluate the TPR analogously to the supervised setting with the imputations in place of the gold-standard labels as

$$\widetilde{\text{TPR}}_{\text{ssROC}}(c) = \frac{\sum_{i=n+1}^{n+N} \hat{m}(S_i) I(S_i > c)}{\sum_{i=n+1}^{n+N} \hat{m}(S_i)}.$$

Figure 3: **Two steps of ssROC using the true positive rate (TPR) as an example.**

resampling procedure in Supplementary Section 1. In Supplementary Section 2, we also provide a brief theoretical justification for the improved efficiency of ssROC relative to supROC for a wide variety of weakly-supervised PAs. Our analysis verifies that ssROC is guaranteed to have lower variance than its supervised counterpart.

Data and metrics for evaluation

We assessed the performance of ssROC using both simulated and real-world EHR data from MGB.

Simulation study

We considered two settings that mimic scenarios with low and high PA accuracy. In both settings, Y is generated from a logistic regression model based on p covariates,

$\mathbf{X} = (X_1, \dots, X_p)$. We generated \mathbf{X} from a multivariate normal distribution with each component of the mean vector determined by a $\text{Bin}(3, 0.3)$ random variable and a compound symmetric covariance structure with a variance of 3 and covariance of 0.6. The two settings are as follows:

- **Setting 1: PA with low accuracy.** Y is generated from the logistic regression model $P(Y = 1 \mid \mathbf{X}) = \frac{1}{1 + \exp\{-(0.1X_1 + 0.1X_2 + 0.2X_1X_2)\}}$. The PA score is generated using the linear predictor of the logistic regression model excluding the interaction term so that $S = \frac{1}{1 + \exp\{-(0.1X_1 + 0.1X_2)\}}$. In this setting, the AUC of S for Y is 67.5.
- **Setting 2: PA with high accuracy.** Y is generated from the logistic regression model $P(Y = 1 \mid \mathbf{X}) = \frac{1}{1 + \exp\{-(-4 + X_1 + X_2 + 0.5X_3 + 0.5X_4)\}}$. The PA score is generated using the linear predictor of the logistic regression model so that $S = \frac{1}{1 + \exp\{-(-4 + X_1 + X_2 + 0.5X_3 + 0.5X_4)\}}$. In this setting, the AUC of S for Y is 95.3.

In both settings, we let the size of the unlabeled data be $N = 10,000$ and varied the labeled size as $n = 100$ and 200 , resulting in a total of 4 simulation studies. We summarize results across 2,000 simulated datasets for each study.

Real-world EHR data application

We validated our method using real-world EHR data from MGB, a Boston-based health-care system anchored by two tertiary care centers, Brigham and Women’s Hospital and Massachusetts General Hospital. We evaluated the PAs for seven phenotypes, including Breast Cancer (BrCa), Coronary Artery Disease (CAD), Depression, Epilepsy, Hypertension (HTN), Type 1 Diabetes Mellitus (T1DM), and Type 2 Diabetes Mellitus (T2DM) from the MGB Biobank. This biobank contains linked EHR and genetic data from MGB between 1990 and 2015. We also evaluated an algorithm for Pseudogout (pGout) from

the Research Patient Data Registry of MGB, which stores data on over 1 billion visits containing diagnoses, medications, procedures, laboratory information, and clinical notes from 1991 to 2017.

The underlying full data for each phenotype consisted of patient records with at least one phenotype-related PheCode in their record [47]. A subset of patients was randomly sampled from the full data and sent for chart review. The average size of the labeled and unlabeled data were 226 and 6,700, respectively. For each phenotype, the PA was obtained by fitting PheNorm without the random corruption denoising step. PheNorm is a recently proposed weakly-supervised method based on normalizing silver-standard labels with respect to patient healthcare utilization and is described in detail in Supplementary Section 3 [48]. The silver-standard labels were taken as the total numbers of (i) phenotype-related PheCodes and (ii) positive mentions of the phenotype-related clinical concepts in patient records. Clinical concepts were extracted from clinical notes with the Narrative Information Linear Extraction and mapped to concept unique identifiers (CUIs) in the Unified Medical Language System [49, 50]. The phenotypes represent varying levels of PA accuracy, differences in labeled and unlabeled dataset sizes (n and N , respectively), and prevalence (P). A summary of the eight phenotypes is presented in Table 1.

Benchmark method and reported metrics

We compared the PA evaluation results from ssROC and the benchmark, supROC, using the real and simulated data. To improve the performance of the local constant regression step, we transformed the PA scores by their empirical cumulative distribution function [51]. We used the Gaussian kernel with the bandwidth determined by the standard de-

Phenotype	n	N	P	PheCode	CUI
Breast Cancer (BrCa)	94	2002	0.78	174	C0006142
Coronary Artery Disease (CAD)	186	3793	0.37	411.4	C0010054
Depression	252	10,189	0.55	296.2	C0011581
Epilepsy	117	2225	0.48	345.1	C0014544
Hypertension (HTN)	390	19,853	0.79	401	C0020538
pGout	365	12,035	0.22	274	C0263708
Type 1 Diabetes Mellitus (T1DM)	128	2111	0.16	250.1	C0011854
Type 2 Diabetes Mellitus (T2DM)	280	3460	0.36	250.2	C0011860

Table 1: **Summary of the MGB Phenotypes.** The labeled dataset size (n), the unlabeled dataset size (N), and the prevalence (P) of the eight phenotypes as well as the main PheCode and concept unique identifier (CUI) used to train PheNorm. The underlying full data for each phenotype included all participants who passed the filter of ≥ 1 PheCode for the phenotype of interest.

viation of the standardized PA scores divided by $n^{0.45}$ [38]. We obtained standard error estimates for the ROC parameters using perturbation resampling with 500 replications and used weights sampled from a scaled beta distribution given by $4 \cdot \text{Beta}(1/2, 3/2)$ to improve finite-sample performance [52]. We focused on logit-based confidence intervals (CIs) due to their improved performance relative to standard Wald intervals [53]. To obtain the logit-based intervals, we applied a logit transformation to the resampled estimates, computed a Wald-based interval with the transformed estimates, and then converted the upper and lower confidence bounds back to the original scale.

In simulations, the ground truth was the median of the ROC estimates using the completely labeled data across the replicated datasets. We assessed percent bias for both supROC and ssROC by computing the median of $[(\text{point estimate} - \text{ground truth}) / \text{ground truth}] \times 100$ across the simulated datasets. We also computed the empirical standard error (ESE) as the standard deviation of the estimates across the replicated datasets

and the asymptotic standard error (ASE) as the median of the standard error estimates from the perturbation resampling procedure across the replicated datasets. Using mean squared error (MSE) as an aggregate measure of bias and variance, we evaluated the relative efficiency (RE) as the ratio of the MSE of supROC to the MSE of ssROC. The performance of our resampling procedure was assessed with the coverage probability (CP) of the 95% CIs for both estimation procedures. In the real data analysis, we present point estimates from both supROC and ssROC and the RE defined as the ratio of the variance of supROC to ssROC. We evaluated the performance of the PAs at an FPR of 10% and report the results for the AUC, classification threshold (Threshold), TPR, PPV, and NPV for both the real and simulated data.

RESULTS

Simulation

We present point estimates and percent biases for the ROC parameters at an FPR of 10% for both simulation settings in Table 2. Both supROC and ssROC showed minimal bias across all ROC parameters, labeled dataset sizes, and simulation settings. The RE of ssROC compared to supROC is illustrated in Figure 4 with a median RE of 1.2 for low PA accuracy (setting 1) and 1.5 for high PA accuracy (setting 2). The higher gain in efficiency in setting 2 coincides with our theoretical result and highlights the benefits of ssROC relative to supROC, particularly when the PA is highly informative of the gold-standard label.

The most substantial improvements in the RE are observed for PPV. For example, in setting 2 with $n = 200$, the RE for PPV is 2.3. Practically, an RE exceeding 1 indicates that ssROC has a smaller variance than supROC (assuming the point estimates from the

two procedures are comparable). One may also view a reduction in variance in terms of the sample size required for ssROC to achieve the same variance as supROC. Again using PPV as an example, an RE of 2.3 suggests that ssROC with $n = 87$ can achieve the same variance as supROC with $n = 200$. Supplementary Table 2 supports this observation, indicating that the ASE of the PPV from ssROC with $n = 100$ is lower than the ESE from supROC with $n = 200$ (2.0 vs. 2.2).

Supplementary Tables 1 and 2 present the ESE, ASE, and CP of the 95% CIs for simulation settings 1 and 2, respectively. The proposed logit-based CI consistently achieved coverage close to the nominal level for both methods across all settings and parameters. The tables also illustrate the benefit of the logit-based interval over the standard Wald interval. For example, in setting 2 with $n=100$, the CPs of Wald CIs for AUC are 90.1% (supROC) and 89.5% (ssROC), while the CPs of the logit-based intervals are 96.9% and 93.5%.

n	Method	AUC		Threshold		TPR		PPV		NPV	
		Est.	%Bias	Est.	%Bias	Est.	%Bias	Est.	%Bias	Est.	%Bias
Setting 1											
100	supROC	67.48	-0.02	73.93	-0.15	37.05	1.11	84.63	0.00	48.66	0.39
	ssROC	67.55	0.14	73.84	-0.14	37.18	1.13	84.59	-0.03	48.84	0.62
200	supROC	67.45	0.04	73.87	-0.01	36.90	0.70	84.33	0.03	48.70	0.24
	ssROC	67.56	0.16	73.87	-0.09	36.91	0.21	84.36	0.01	48.78	0.30
Setting 2											
100	supROC	95.27	0.22	61.58	0.46	84.68	0.43	83.69	-0.02	90.53	0.24
	ssROC	95.10	0.02	61.55	0.36	84.36	-0.51	83.79	-0.14	90.37	-0.21
200	supROC	95.30	0.12	61.48	0.25	85.08	0.47	83.85	-0.04	90.77	0.25
	ssROC	95.24	0.01	61.46	0.22	84.92	0.06	83.86	-0.15	90.71	0.02

Table 2: **Point estimates and percent bias for both simulation settings at a FPR of 10%.** For both settings, the size of the unlabeled was $N = 10,000$.

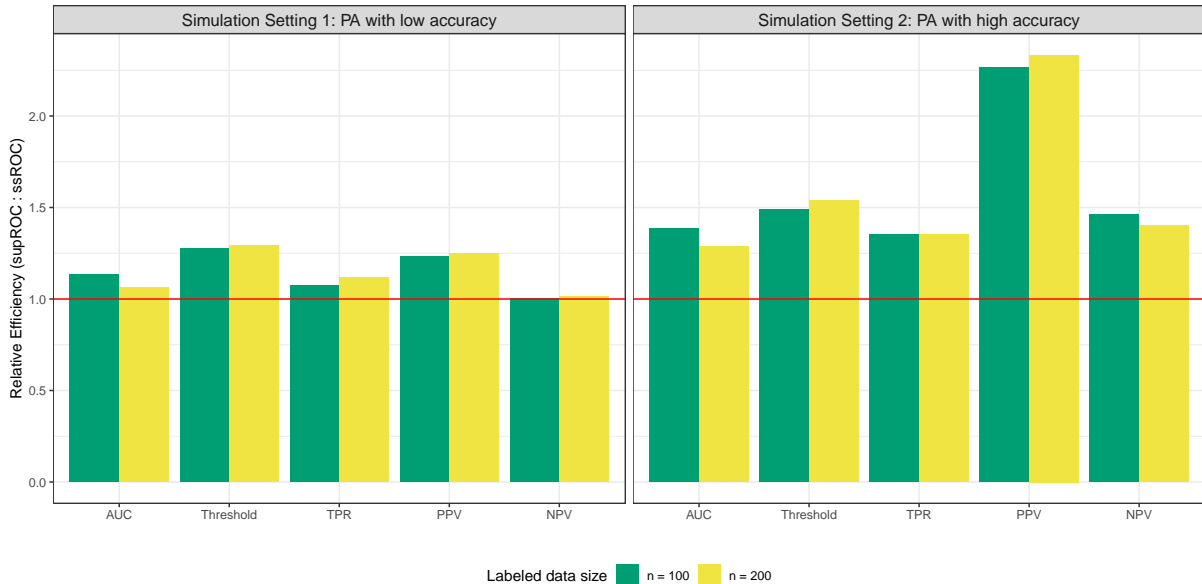


Figure 4: **Relative efficiency for both simulation settings at a FPR of 10%.** Relative efficiency is defined as the mean squared error of supROC compared to the mean squared error of ssROC. For both settings, the size of the unlabeled was $N = 10,000$.

Analysis of eight PAs from MGB

Figure 5 displays the point estimates for the eight phenotypes from MGB at a FPR of 10%. The top row contains the PAs with lower accuracy. Generally, the point estimates from ssROC are similar to those from supROC. However, there are some differences in the classification threshold estimates for Depression, HTN, and CAD, which leads to some discrepancies in the corresponding point estimates for the TPR, PPV, and NPV. As supROC is only evaluated at the unique PA scores in the labeled dataset, the threshold estimate can be unstable at some FPRs. In contrast, ssROC evaluates the ROC parameters across a broader range of PA scores in the larger unlabeled dataset and results in a more stable estimation. Despite these differences, it is important to note that the 95% CIs for all estimators consistently overlapped, as shown in Supplementary Figure 1.

Figure 6 shows the median RE of supROC to ssROC across the eight phenotypes at a FPR of 10%. The median RE gain across phenotypes and metrics was 1.7, implying that ssROC can achieve the same precision as supROC, but with roughly 60% of the amount of data on average. Consistent with the simulation findings, the most significant RE gain was observed in PPV followed by the classification threshold, with median RE both near 2.1. The lowest gain was in AUC, with a median RE of 1.2. These results suggest that ssROC can achieve equivalent precision to supROC with respect to PPV with approximately 52% of the labeled data and maintain equivalent precision for AUC with 15% less labeled data. Additionally, Depression and HTN exhibited very high RE for the classification threshold (Supplementary Figure 2). This behavior further emphasizes the stability of ssROC relative to supROC in real data. For instance, Supplementary Figure 3 illustrates that the empirical distribution of the resampled estimates from supROC is skewed for Depression and multimodal for HTN due to the aforementioned difficulties in estimating the classification threshold with the small amount of labeled data.

Consistent with our simulation and theoretical results, we also observe that RE is linked to PA accuracy. For example, a phenotype with high PA accuracy, such as BrCa (AUC = 94.4), has a median RE of 2.2 while pGout, an episodic disease without a specific billing code, has the lowest PA accuracy (AUC = 61.4) and a median RE near 1. These findings underscore the advantages of our proposed ssROC method compared to its supervised counterpart: (i) ssROC increases precision when the PA score is predictive and (ii) performs on par with the supROC when the PA score is uninformative.

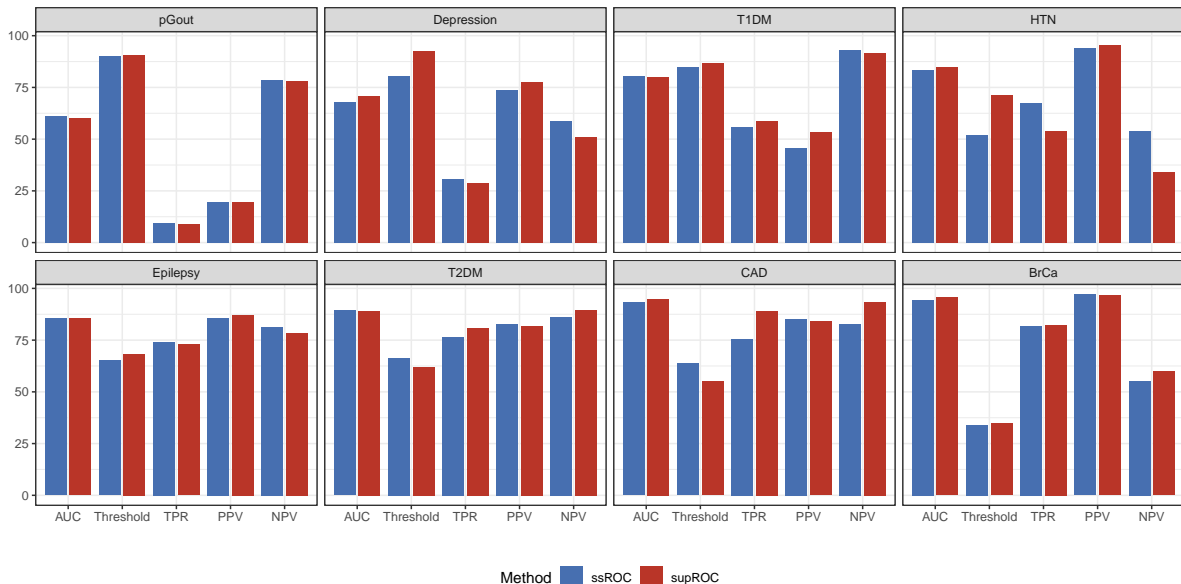


Figure 5: **Point estimates for the 8 phenotypes from MGB at a FPR of 10%.** Point estimates of the ROC parameters for both ssROC and supROC.

DISCUSSION

Although high-throughput phenotyping is the backbone of EHR-based research, there is a paucity of methods for reliably evaluating the predictive performance of a PA with limited labeled data. The proposed ssROC method fills this gap. ssROC is a simple two-step estimation procedure that leverages large volumes of unlabeled data by imputing missing gold-standard labels with a nonparametric recalibration of a PA score. Unlike existing procedures for PA evaluation in the informatics literature, ssROC eliminates the requirement that the PA be properly calibrated to yield unbiased estimation of the ROC parameters and may be utilized for ML-based PAs [25, 37]. While we focus specifically on weakly-supervised PAs in our theoretical analysis and real data example, given their increasing popularity and ability to automate PA estimation, ssROC can also be used to evaluate rule-based or other ML-based PAs. Moreover, by harnessing unlabeled data,

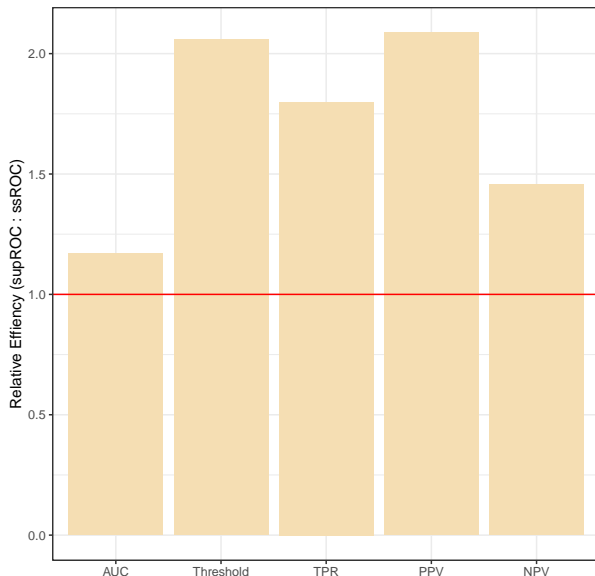


Figure 6: **Relative efficiency for the 8 phenotypes from MGB at a FPR of 10%.** The median relative efficiency (RE) of supROC versus ssROC across the 8 phenotypes. RE is defined as the ratio of the variance of the estimates from supROC and the variance of the estimates from ssROC.

ssROC yields substantially less variable estimates than supROC in both simulated and real data. Practically, this translates into a significant reduction in the amount of chart review required to obtain a precise understanding of PA performance.

While our work is a first step toward streamlining PA evaluation, there are several avenues for future research. First, ssROC assumes that the labeled examples have been randomly sampled from the underlying full data. More effective sampling strategies, such as targeted or stratified sampling, have the potential to further improve upon the efficiency of ssROC, but require future research [54]. Secondly, the nonparametric recalibration step demands a sufficient amount of labeled data for the local constant regression to be well estimated. Our future work will develop a flexible parametric recalibration procedure that accommodates smaller labeled data sizes. Thirdly, ssROC can also be extended for

model comparisons and evaluation of fairness metrics, which are urgently needed given the increasing recognition of algorithmic unfairness in informatics applications. The recalibration step would need to be augmented in both settings to utilize additional information in multiple PA scores or protected attributes, respectively. This augmentation could lead to a potentially more efficient procedure as ssROC currently only uses information from one PA score for imputation. Lastly, our results demonstrate the ability of ssROC to provide accurate phenotyping for eight phenotypes with variable prevalence, labeled and unlabeled dataset sizes, and PA performance within one health system. Further work is needed to understand the performance of our method across a diverse range of phenotypes and to extend our approach to accommodate federated analyses across multiple healthcare systems.

CONCLUSION

In this paper, we introduced a semi-supervised approach, called *ssROC*, that leverages a large volume of unlabeled data together with a small subset of gold-standard labeled to precisely estimate the ROC parameters of PAs. PA development involves two key steps: (i) algorithm estimation and (ii) algorithm evaluation. While a considerable amount of effort has been placed on algorithm estimation, *ssROC* fills the current gap in robust methodology for predictive performance evaluation. Additionally, *ssROC* is simple to implement and is available in open-source R software to encourage use in practice. When used in conjunction with weakly-supervised PAs, *ssROC* demonstrates the potential to facilitate the reliable and streamlined phenotyping that is necessary for a wide variety of translational EHR applications.

FUNDING

The project was supported by the Natural Sciences and Engineering Research Council of Canada grant (RGPIN-2021-03734), the University of Toronto Connaught New Researcher Award, and the University of Toronto Seed Funding for Methodologists Grant (to JeG).

AUTHOR CONTRIBUTIONS

JeG conceived and designed the study. JeG, JiG, CB, and CH conducted simulation analyses. CB and CH conducted real data analyses. JeG, JiG, CB, and KZ analyzed and interpreted the results. JeG and JiG drafted and revised the manuscript. All authors reviewed and approved the final manuscript.

CONFLICT OF INTEREST STATEMENT

The authors have no conflicts of interest to declare.

DATA AND CODE AVAILABILITY

Our proposed method is implemented as an R software package, `ssROC`, which is available at <https://github.com/jlgrons/ssROC>.

REFERENCE

1. McGinnis, J. M., Olsen, L., Goolsby, W. A., *et al.* *Clinical data as the basic staple of health learning: Creating and protecting a public good: Workshop summary* (National Academies Press, 2011).
2. Boockvar, K. S., Livote, E. E., Goldstein, N., *et al.* Electronic health records and adverse drug events after patient transfer. *Quality and Safety in Health Care* **19**, e16–e16 (2010).
3. Kurreeman, F., Liao, K., Chibnik, L., *et al.* Genetic basis of autoantibody positive and negative rheumatoid arthritis risk in a multi-ethnic cohort derived from electronic health records. *The American Journal of Human Genetics* **88**, 57–69 (2011).
4. Liao, K. P., Kurreeman, F., Li, G., *et al.* Associations of autoantibodies, autoimmune risk alleles, and clinical diagnoses from the electronic medical records in rheumatoid arthritis cases and non–rheumatoid arthritis controls. *Arthritis & Rheumatism* **65**, 571–581 (2013).
5. Chen, C.-Y., Lee, P. H., Castro, V. M., *et al.* Genetic validation of bipolar disorder identified by automated phenotyping using electronic health records. *Translational psychiatry* **8**, 1–8 (2018).
6. Li, R., Chen, Y., Ritchie, M. D., *et al.* Electronic health records and polygenic risk scores for predicting disease risk. *Nature Reviews Genetics*, 1–10 (2020).
7. Brat, G. A., Weber, G. M., Gehlenborg, N., *et al.* International electronic health record-derived COVID-19 clinical course profiles: the 4CE consortium. *NPJ digital medicine* **3**, 1–9 (2020).

8. Bastarache, L. Using phecodes for research with the electronic health record: from PheWAS to PheRS. *Annual review of biomedical data science* **4**, 1–19 (2021).
9. Prieto-Alhambra, D., Kostka, K., Duarte-Salles, T., *et al.* Unraveling COVID-19: a large-scale characterization of 4.5 million COVID-19 cases using CHARYBDIS. *Research square* (2021).
10. Henry, K. E., Adams, R., Parent, C., *et al.* Factors driving provider adoption of the TREWS machine learning-based early warning system and its effects on sepsis treatment timing. *Nature medicine* **28**, 1447–1454 (2022).
11. Shivade, C., Raghavan, P., Fosler-Lussier, E., *et al.* A review of approaches to identifying patient phenotype cohorts using electronic health records. *Journal of the American Medical Informatics Association* **21**, 221–230 (2014).
12. Banda, J. M., Seneviratne, M., Hernandez-Boussard, T., *et al.* Advances in electronic phenotyping: from rule-based definitions to machine learning models. *Annual review of biomedical data science* **1**, 53 (2018).
13. Alzoubi, H., Alzubi, R., Ramzan, N., *et al.* A review of automatic phenotyping approaches using electronic health records. *Electronics* **8**, 1235 (2019).
14. Yang, S., Varghese, P., Stephenson, E., *et al.* Machine learning approaches for electronic health records phenotyping: a methodical review. *Journal of the American Medical Informatics Association* **30**, 367–381 (2023).
15. Zhang, Y., Cai, T., Yu, S., *et al.* High-throughput phenotyping with electronic medical record data using a common semi-supervised approach (PheCAP). *Nature Protocols* **14**, 3426–3444 (2019).
16. Murphy, S., Churchill, S., Bry, L., *et al.* Instrumenting the health care enterprise for discovery research in the genomic era. *Genome research* **19**, 1675–1681 (2009).

17. Castro, V., Shen, Y., Yu, S., *et al.* Identification of subjects with polycystic ovary syndrome using electronic health records. *Reproductive Biology and Endocrinology* **13**, 116 (2015).
18. Teixeira, P. L., Wei, W.-Q., Cronin, R. M., *et al.* Evaluating electronic health record data sources and algorithmic approaches to identify hypertensive individuals. *Journal of the American Medical Informatics Association* **24**, 162–171 (Jan. 2017).
19. Geva, A., Gronsbell, J. L., Cai, T., *et al.* A computable phenotype improves cohort ascertainment in a pediatric pulmonary hypertension registry. *The Journal of pediatrics* **188**, 224–231 (2017).
20. Meaney, C., Widdifield, J., Jaakkimainen, L., *et al.* Using Biomedical Text as Data and Representation Learning for Identifying Patients with an Osteoarthritis Phenotype in the Electronic Medical Record. *International Journal of Population Data Science* **3** (2018).
21. Gehrman, S., Deroncourt, F., Li, Y., *et al.* Comparing deep learning and concept extraction based methods for patient phenotyping from clinical narratives. *PLOS ONE* **13** (ed Chuang, J.-H.) e0192360 (Feb. 2018).
22. Liao, K. P., Sun, J., Cai, T. A., *et al.* High-throughput multimodal automated phenotyping (MAP) with application to PheWAS. *Journal of the American Medical Informatics Association* **26**, 1255–1262 (2019).
23. Nori, V. S., Hane, C. A., Sun, Y., *et al.* Deep neural network models for identifying incident dementia using claims and EHR datasets. *PLOS ONE* **15** (ed Chen, K.) e0236400 (Sept. 2020).

24. Ni, Y., Bachtel, A., Nause, K., *et al.* Automated detection of substance use information from electronic health records for a pediatric population. *Journal of the American Medical Informatics Association* **28**, 2116–2127 (2021).
25. Swerdel, J. N., Hripcsak, G. & Ryan, P. B. PheValuator: development and evaluation of a phenotype algorithm evaluator. *Journal of biomedical informatics* **97**, 103258 (2019).
26. Chartier, C., Gfrerer, L. & Austen, W. G. ChartSweep: A HIPAA-compliant Tool to Automate Chart Review for Plastic Surgery Research. *Plastic and Reconstructive Surgery - Global Open* **9**, e3633. (2023) (2021).
27. Yu, S., Liao, K. P., Shaw, S. Y., *et al.* Toward high-throughput phenotyping: unbiased automated feature extraction and selection from knowledge sources. *Journal of the American Medical Informatics Association* **22**, 993–1000 (2015).
28. Yu, S., Chakraborty, A., Liao, K. P., *et al.* Surrogate-assisted feature extraction for high-throughput phenotyping. *Journal of the American Medical Informatics Association* **24**, e143–e149 (2017).
29. Nogues, I.-E., Wen, J., Lin, Y., *et al.* Weakly Semi-supervised phenotyping using Electronic Health records. *Journal of Biomedical Informatics* **134**, 104175 (2022).
30. Wright, A., Chen, E. S. & Maloney, F. L. An automated technique for identifying associations between medications, laboratory results and problems. *Journal of biomedical informatics* **43**, 891–901 (2010).
31. Wright, A., Pang, J., Feblowitz, J. C., *et al.* A method and knowledge base for automated inference of patient problems from structured data in an electronic medical record. *Journal of the American Medical Informatics Association* **18**, 859–867 (2011).

32. Agarwal, V., Podchiyska, T., Banda, J. M., *et al.* Learning statistical models of phenotypes using noisy labeled training data. *Journal of the American Medical Informatics Association* **23**, 1166–1173 (2016).
33. Banda, J. M., Halpern, Y., Sontag, D., *et al.* Electronic phenotyping with APHRODITE and the Observational Health Sciences and Informatics (OHDSI) data network. *AMIA Summits on Translational Science Proceedings* **2017**, 48 (2017).
34. Huang, J., Duan, R., Hubbard, R. A., *et al.* PIE: A prior knowledge guided integrated likelihood estimation method for bias reduction in association studies using electronic health records data. *Journal of the American Medical Informatics Association* **25**, 345–352 (2018).
35. Tong, J., Huang, J., Chubak, J., *et al.* An augmented estimation procedure for EHR-based association studies accounting for differential misclassification. *Journal of the American Medical Informatics Association* **27**, 244–253 (2020).
36. Yin, Z., Tong, J., Chen, Y., *et al.* A cost-effective chart review sampling design to account for phenotyping error in electronic health records (EHR) data. *Journal of the American Medical Informatics Association* **29**, 52–61 (2022).
37. Swerdel, J. N., Schuemie, M., Murray, G., *et al.* PheValuator 2.0: Methodological improvements for the PheValuator approach to semi-automated phenotype algorithm evaluation. *Journal of Biomedical Informatics* **135**, 104177 (2022).
38. Gronsbell, J. L. & Cai, T. Semi-supervised approaches to efficient evaluation of model prediction performance. *Journal of the Royal Statistical Society: Series B (Statistical Methodology)* **80**, 579–594 (2018).

39. Gronsbell, J., Liu, M., Tian, L., *et al.* Efficient estimation and evaluation of prediction rules in semi-supervised settings under stratified sampling. *arXiv preprint arXiv:2010.09443* (2020).
40. Van Calster, B., McLernon, D. J., Van Smeden, M., *et al.* Calibration: the Achilles heel of predictive analytics. *BMC medicine* **17**, 1–7 (2019).
41. Huang, Y., Li, W., Macheret, F., *et al.* A tutorial on calibration measurements and calibration models for clinical prediction models. *Journal of the American Medical Informatics Association* **27**, 621–633 (2020).
42. Pepe, M. S. *The statistical evaluation of medical tests for classification and prediction* (Oxford University Press, 2003).
43. Cai, T. & Moskowitz, C. S. Semi-parametric estimation of the binormal ROC curve for a continuous diagnostic test. *Biostatistics* **5**, 573–586 (2004).
44. Jin, Z., Ying, Z. & Wei, L. A Simple Resampling Method by Perturbing the Minimax. *Biometrika* **88**, 381–390 (June 2001).
45. Bertail, P., Cléménçon, S. & Vayatis, N. On bootstrapping the ROC curve. *Advances in Neural Information Processing Systems* **21** (2008).
46. Newey, W., Hsieh, F. & Robins, J. *Undersmoothing and Bias Corrected Functional Estimation* Working papers 98-17 (Massachusetts Institute of Technology (MIT), Department of Economics, 1998). <https://EconPapers.repec.org/RePEc:mit:worpap:98-17>.
47. Denny, J. C., Bastarache, L., Ritchie, M. D., *et al.* Systematic comparison of phenome-wide association study of electronic medical record data and genome-wide association study data. *Nature biotechnology* **31**, 1102–1111 (2013).

48. Yu, S., Ma, Y., Gronsbell, J., *et al.* Enabling phenotypic big data with PheNorm. *Journal of the American Medical Informatics Association* **25**, 54–60 (2018).
49. Lindberg, D. A., Humphreys, B. L. & McCray, A. T. The unified medical language system. *Yearbook of medical informatics* **2**, 41–51 (1993).
50. Yu, S., Cai, T. & Cai, T. NILE: fast natural language processing for electronic health records. *arXiv preprint arXiv:1311.6063* (2013).
51. Wand, M. P., Marron, J. S. & Ruppert, D. Transformations in density estimation. *Journal of the American Statistical Association* **86**, 343–353 (1991).
52. Sinnott, J. A. & Cai, T. Inference for survival prediction under the regularized Cox model. *Biostatistics* **17**, 692–707 (2016).
53. Agresti, A. *Categorical data analysis* (John Wiley & Sons, 2012).
54. Tan, W. K. & Heagerty, P. J. Surrogate-guided sampling designs for classification of rare outcomes from electronic medical records data. *Biostatistics* **23**, 345–361 (2022).

ssROC: Semi-Supervised ROC Analysis for Reliable and Streamlined Evaluation of Phenotyping Algorithms

Jianhui Gao[†], Clara-Lea Bonzel[†], Chuan Hong,
Paul Varghese, Karim Zakir, Jessica Gronsbell*

[†] These authors contributed equally.

*Correspondence: j.gronsbell@utoronto.ca.

Contents

1	Inference Procedure for ssROC	1
1.1	Perturbation Resampling Procedure	1
1.2	Construction of Confidence Intervals (CIs)	2
2	Theoretical Properties of ssROC and supROC	4
2.1	Proof of Theorem 1	7
2.1.1	Supervised Estimator	7
2.2	Semi-supervised Estimator	11
3	Description of the PheNorm Algorithm	16
4	Simulation Study	18
5	Analysis of Eight PAs from MGB	20
5.1	Confidence Intervals	20

5.2	Relative Efficiency	21
5.3	Perturbation Resampling	22

1 Inference Procedure for ssROC

We detail the perturbation resampling procedure for obtaining standard error estimates and also describe the construction of the corresponding confidence (CI) interval.

1.1 Perturbation Resampling Procedure

Perturbation resampling involves obtaining a large number, B , of perturbed estimates of the parameter of interest by re-weighting the observations according to independently and identically distributed non-negative weights generated independently from the data and from a distribution with unit mean and variance [1]. Perturbation can be thought of as a smoothed version of traditional bootstrap resampling. In a bootstrap resample, one is essentially re-weighting each observation by weight from a multinomial random variable with the number of trials equal to the sample size and the probabilities all equal to the inverse of the sample size. Perturbation resampling can exhibit improved coverage relative to the traditional bootstrap using weights from a distribution of a continuous random variable [1].

Specifically, we let $\mathcal{G}^{(b)} = \{G_1^{(b)}, \dots, G_n^{(b)}, G_{n+1}^{(b)}, \dots, G_{n+N}^{(b)}\}$ be a set of independent and identically distributed positive random variables with unit mean and variance for $b = 1, \dots, B$. Using the TPR for illustration, perturbation resampling involves iterating the following procedure B times:

Step I. Obtain a perturbed estimate of the $m(s) = P(Y = 1 \mid S = s)$ as

$$\hat{m}^{(b)}(s) = \frac{\sum_{i=1}^n K_h(S_i - s) Y_i G_i^{(b)}}{\sum_{i=1}^n K_h(S_i - s) G_i^{(b)}}$$

using the same kernel and bandwidth for the original data.

Step II. Obtain a perturbed estimate of the TPR as

$$\widehat{\text{TPR}}_{ssROC}^{(b)}(c) = \frac{\sum_{i=n+1}^{n+N} \widehat{m}^{(b)}(S_i) I(S_i > c) G_i^{(b)}}{\sum_{i=n+1}^{n+N} \widehat{m}^{(b)}(S_i) G_i^{(b)}}.$$

The same procedure can be applied to all of the ROC parameters. Additionally, it is important to note that theoretically one does not need to apply weights to Step II as we assume $n \gg N$. This assumption implies that integrating over the empirical distribution of the PA scores in the unlabeled set does not contribute to the overall variation in the ROC parameter estimates [2]. However, we found that using weights for both Step I and Step II provided improved coverage in our simulation studies. We used an analogous procedure for supROC.

1.2 Construction of Confidence Intervals (CIs)

Analogous to bootstrap resampling, the standard error estimates ($\widehat{\text{se}}$) are obtained with the standard deviation of the B perturbed TPR parameter estimates as

$$\widehat{\text{se}} \left[\widehat{\text{TPR}}_{ssROC}(c) \right] = \sqrt{\frac{1}{B-1} \sum_{b=1}^B \left[\widehat{\text{TPR}}_{ssROC}^{(b)}(c) - \frac{1}{B} \sum_{b=1}^B \widehat{\text{TPR}}_{ssROC}^{(b)}(c) \right]^2}.$$

Relying on the normal approximation to the sampling distribution of the ssROC estimator of the TPR, a standard Wald $100(1 - \alpha)\%$ CI can be constructed accordingly as $\widehat{\text{TPR}}_{ssROC}(c) \pm z_{1-\alpha/2} \times \widehat{\text{se}} \left[\widehat{\text{TPR}}_{ssROC}(c) \right]$. We verify in the next section that all of the ssROC parameters are asymptotically normal.

However, analogously to supervised estimation, the sampling distribution of the ROC parameters are often skewed when the size of the labeled data is not large [3]. Logit-based intervals can improve the coverage of the CI. The logit-based intervals are obtained by applying a logit transformation to the resampled estimates, computing a Wald-based

interval with the transformed estimates, and then converting the upper and lower confidence bounds back to the original scale.

Specifically, we apply $\text{logit}(x) = \log\left(\frac{x}{1-x}\right)$ to $\widehat{\text{TPR}}_{ssROC}(c)$, and a $100(1 - \alpha)\%$ Wald CI of $\text{logit}\left[\widehat{\text{TPR}}_{ssROC}(c)\right]$ is

$$\text{logit}\left[\widehat{\text{TPR}}_{ssROC}(c)\right] \pm z_{1-\alpha/2} \times \widehat{\text{se}}\left\{\text{logit}\left[\widehat{\text{TPR}}_{ssROC}(c)\right]\right\},$$

where $\widehat{\text{se}}\left\{\text{logit}\left[\widehat{\text{TPR}}_{ssROC}(c)\right]\right\}$ is the standard deviation of the B perturbed logit transformed estimates. To obtain a $100(1 - \alpha)\%$ CI for $\widehat{\text{TPR}}_{ssROC}(c)$, we convert the upper and lower confidence bounds back by

$$\text{logit}^{-1}\left\{\text{logit}\left[\widehat{\text{TPR}}_{ssROC}(c)\right] \pm z_{1-\alpha/2} \times \widehat{\text{se}}\left\{\text{logit}\left[\widehat{\text{TPR}}_{ssROC}(c)\right]\right\}\right\},$$

where $\text{logit}^{-1}(x) = \frac{1}{1+\exp(-x)}$. We recommend the use the logit-based interval as it performed best overall in terms of coverage probability in our simulation studies.

2 Theoretical Properties of ssROC and supROC

We present the asymptotic distributions of ssROC and supROC and also compare their asymptotic variances to establish the improved precision of ssROC relative to supROC. The consistency of both estimators follows from [2]. Most of our assumptions are adopted from [2], which are restated below.

Assumption 1 (Semi-supervised setting). *We assume that: (i) $\mathcal{L} \perp\!\!\!\perp \mathcal{U}$, (ii) $N \gg n$ so that $n/N \rightarrow 0$ as $n \rightarrow \infty$, and (iii) the labels are missing completely at random.*

Assumption 2 (Modeling Assumptions for the Phenotyping Algorithm (PA) score). *We assume that the PA score is derived from a working parametric model fit with \mathcal{U} . The model is parameterized by a p -dimensional parameter, $\boldsymbol{\theta}$, for some fixed p . Let $\hat{\boldsymbol{\theta}}$ be the estimator obtained from the fitting with \mathcal{U} and let $\boldsymbol{\theta}^*$ be the limiting value of $\hat{\boldsymbol{\theta}}$ where $\boldsymbol{\theta}^*$ belongs to a compact parameter space. We assume that $\hat{\boldsymbol{\theta}}$ is asymptotically linear with*

$$\sqrt{N}(\hat{\boldsymbol{\theta}} - \boldsymbol{\theta}^*) = N^{-1/2} \sum_{i=1}^N U(\mathbf{Z}_i) + o_p(1)$$

where \mathbf{Z}_i denotes the data used for algorithm estimation, $U(\cdot)$ is a deterministic function with $\| \text{Var}[U(\mathbf{Z}_i)] \| < \infty$ and $E[U(\mathbf{Z}_i)] = 0$. For ease of notation and consistency with the main text, we denote the estimated PA score as $S = S_{\hat{\boldsymbol{\theta}}} = S(\mathbf{Z}; \hat{\boldsymbol{\theta}})$ and the limiting PA score $S^* = S_{\boldsymbol{\theta}^*} = S(\mathbf{Z}; \boldsymbol{\theta}^*)$. We assume that S^* is a continuous random variable with continuously differentiable density function, $f(s)$, with bounded support.

Remark. The assumptions on the model used to obtain the PA are quite flexible and include a wide range of commonly used parametric models. For example, the PheNorm algorithm satisfies Assumption 2 [4, 5]. Noisy-label regression models, such as those in APHRODITE, also satisfy Assumption 2 [6, 7].

Assumption 3 (Regularity conditions for kernel smoothing). *We assume that: (i) $K(\cdot)$ is a symmetric q th order kernel for some integer $q \geq 2$ that is bounded and Lipschitz*

continuous, (ii) for some $\epsilon > 0$, $E|Y|^{2+\epsilon} < \infty$ and $\sup_s \int |y|^{2+\epsilon} f(y | s) f(s) dy < \infty$, and (iii) the bandwidth h satisfies $\frac{\log(n)}{n^{1/2}h} \rightarrow 0$ and $n^{1/2}h^2 \rightarrow 0$.

Assumption 4 (Assumptions for ROC analysis). *We assume that for any classification threshold c , the gradient vectors $\nabla_{\theta} \text{TPR}(c)$ and $\nabla_{\theta} \text{FPR}(c)$ exist and are continuous in an open neighbourhood containing θ^* .*

The subsequent discussions are abbreviated versions of the arguments provided in [2] and are provided to facilitate our comparison of ssROC relative to supROC. The primary difference in our analysis is that we assume a more flexible working model based on a weakly-supervised estimation, while [2] assumes a supervised penalized logistic regression model with the ALASSO penalty.

We provide the influence function for a point along the ROC curve, $\text{ROC}(u_0) = \text{TPR}(c_{u_0})$ where $c_{u_0} = \text{FPR}^{-1}(u_0)$. The corresponding ssROC and supROC are denoted respectively as

$$\widehat{\text{ROC}}_{\text{ssROC}}(u_0) = \widehat{\text{TPR}}_{\text{ssROC}}(\tilde{c}_{u_0}) = \widehat{\text{TPR}}_{\text{ssROC}} \left[\widehat{\text{FPR}}_{\text{ssROC}}^{-1}(u_0) \right]$$

and

$$\widehat{\text{ROC}}_{\text{supROC}}(u_0) = \widehat{\text{TPR}}_{\text{supROC}}(\hat{c}_{u_0}) = \widehat{\text{TPR}}_{\text{supROC}} \left[\widehat{\text{FPR}}_{\text{supROC}}^{-1}(u_0) \right].$$

Our main result is provided in the following theorem.

Theorem 1. *Under Assumption 1 – 4,*

$$\begin{aligned} \widetilde{\mathcal{W}}_{\text{ROC}}(u_0) &= n^{1/2} \left[\widehat{\text{ROC}}_{\text{ssROC}}(u_0) - \text{ROC}(u_0) \right] \\ &= n^{-1/2} \sum_{i=1}^n \mathcal{G}_i(S; \theta^*, c_{u_0}) [Y_i - m(S_i^*)] + o_p(1) \end{aligned}$$

and

$$\begin{aligned}\widehat{W}_{ROC}(u_0) &= n^{1/2} \left[\widehat{ROC}_{supROC}(u_0) - ROC(u_0) \right] \\ &= n^{-1/2} \sum_{i=1}^n [\mathcal{G}_i(S; \boldsymbol{\theta}^*, c_{u_0})(Y_i - \mu) + \Gamma_i(S; \boldsymbol{\theta}^*, c_{u_0})] + o_p(1),\end{aligned}$$

where $\mu = P(Y = 1)$, $R\dot{O}C(u_0) = \frac{\partial ROC(u)}{\partial u}|_{u=u_0}$, $\mathcal{G}_i(S; \boldsymbol{\theta}^*, c_{u_0}) = \left[\mu^{-1} + \mu_0^{-1} R\dot{O}C(u_0) \right] I(S_i^* \geq c_{u_0}) - \left[\mu^{-1} ROC(u_0) + \mu_0^{-1} R\dot{O}C(u_0) u_0 \right]$, and $\Gamma_i(S; \boldsymbol{\theta}^*, c_{u_0}) = I(S_i^* \geq c_{u_0}) - ROC(u_0) - R\dot{O}C(u_0)[I(S_i^* \geq c_{u_0}) - u_0]$.

Remark. Theorem 1 provides the influence functions for the ssROC and supROC estimators. Standard asymptotic theory guarantees both estimators are asymptotically normal with mean $ROC(u_0)$ and variances determined by their influence functions [8]. We use $a\text{Var} \left[\widetilde{ROC}_{ssROC}(u_0) \right]$ and $a\text{Var} \left[\widehat{ROC}_{supROC}(u_0) \right]$ to denote the corresponding asymptotic variances.

Remark. The improvements in $a\text{Var} \left[\widetilde{ROC}_{ssROC}(u_0) \right]$ relative to $a\text{Var} \left[\widehat{ROC}_{supROC}(u_0) \right]$ can be understood from the influence functions in Theorem 1. Specifically, the influence function for ssROC is centered at the conditional mean $m(S_i^*) = P(Y_i = 1 | S_i^*)$ whereas the influence function of supROC is centered at the marginal mean $\mu = P(Y = 1)$. The influence function for supROC also has an extra non-vanishing term $\Gamma_i(S; \boldsymbol{\theta}^*, c_{u_0})$. These differences yield a reduction in the asymptotic variance of ssROC. Additionally, this result differs from that of [2] as the estimated model parameter, $\widehat{\boldsymbol{\theta}}$, converges at a rate of \sqrt{N} . The variation from estimating $\boldsymbol{\theta}^*$ with $\widehat{\boldsymbol{\theta}}$ is therefore asymptotically negligible at the \sqrt{n} rate and hence the proposed semi-supervised estimator *always* has asymptotic variance smaller than that of supROC. Details are provided in Corollary 1.1.

Corollary 1.1. Let $\mathcal{G}(S; \boldsymbol{\theta}^*, c_{u_0}) = \left[\mu^{-1} + \mu_0^{-1} R\dot{O}C(u_0) \right] I(S^* \geq c_{u_0}) - \left[\mu^{-1} ROC(u_0) + \mu_0^{-1} R\dot{O}C(u_0) u_0 \right]$, and $\Gamma(S; \boldsymbol{\theta}^*, c_{u_0}) = I(S^* \geq c_{u_0}) - ROC(u_0) - R\dot{O}C(u_0)[I(S^* \geq c_{u_0}) - u_0]$,

then

$$\begin{aligned}\Delta_v^{asy}(u_0) &:= n \left\{ a \text{Var} \left[\widehat{\text{ROC}}_{supROC}(u_0) \right] - a \text{Var} \left[\widetilde{\text{ROC}}_{ssROC}(u_0) \right] \right\} \\ &= \text{Var} \{ \mathcal{G}(S; \boldsymbol{\theta}^*, c_{u_0}) [m(S^*) - \mu] + \Gamma(S; \boldsymbol{\theta}^*, c_{u_0}) \} \geq 0.\end{aligned}$$

Proof. By the law of total variance,

$$\begin{aligned}n \left\{ a \text{Var} \left[\widehat{\text{ROC}}_{supROC}(c_{u_0}) \right] \right\} &= \\ \text{E} \{ [\mathcal{G}(S; \boldsymbol{\theta}^*, c_{u_0})]^2 \text{Var}(Y|S^*) \} &+ \text{Var} \{ \mathcal{G}(S; \boldsymbol{\theta}^*, c_{u_0}) [m(S^*) - \mu] + \Gamma(S; \boldsymbol{\theta}^*, c_{u_0}) \},\end{aligned}$$

and

$$n \left\{ a \text{Var} \left[\widetilde{\text{ROC}}_{ssROC}(c_{u_0}) \right] \right\} = \text{E} \{ [\mathcal{G}(S; \boldsymbol{\theta}^*, c_{u_0})]^2 \text{Var}(Y|S^*) \}.$$

Hence,

$$\begin{aligned}\Delta_v^{asy}[\text{ROC}(u_0)] &:= n \left\{ a \text{Var} \left[\widehat{\text{ROC}}_{supROC}(u_0) \right] - a \text{Var} \left[\widetilde{\text{ROC}}_{ssROC}(u_0) \right] \right\} \\ &= \text{Var} \{ \mathcal{G}(S; \boldsymbol{\theta}^*, c_{u_0}) [m(S^*) - \mu] + \Gamma(S; \boldsymbol{\theta}^*, c_{u_0}) \} \geq 0.\end{aligned}$$

□

2.1 Proof of Theorem 1

2.1.1 Supervised Estimator

Following the arguments of [2], $\widehat{\text{ROC}}_{supROC}(u_0)$ is consistent for $\text{ROC}(u_0)$ and $\sup_{u_0 \in [0,1]} |\hat{c}_u - c_{u_0}| = o_p(1)$, where $c_{u_0} = \text{FPR}^{-1}(u_0)$, $\hat{c}_u = \widehat{\text{FPR}}_{supROC}^{-1}(u_0)$. To establish the weak con-

vergence of $\widehat{\mathcal{W}}_{\text{ROC}}(u_0) = n^{1/2} \left[\widehat{\text{ROC}}_{\text{supROC}}(u_0) - \text{ROC}(u_0) \right]$, we note that

$$\begin{aligned} \widehat{\mathcal{W}}_{\text{ROC}}(u_0) &= n^{1/2} \left\{ \widehat{\text{TPR}}_{\text{supROC}} \left[\widehat{\text{FPR}}_{\text{supROC}}^{-1}(u_0) \right] - \text{TPR} \left[\text{FPR}^{-1}(u_0) \right] \right\} \\ &= n^{1/2} \left[\widehat{\text{TPR}}_{\text{supROC}}(\hat{c}_u) - \text{TPR}(c_{u_0}) \right] \\ &= n^{1/2} \left[\widehat{\text{TPR}}_{\text{supROC}}(\hat{c}_u) - \text{TPR}(\hat{c}_u) \right] + n^{1/2} [\nabla_c \text{TPR}(c_{u_0})(\hat{c}_u - c_{u_0})] + o_p(1) \\ &= \widehat{\mathcal{W}}_{\text{TPR}}(\hat{c}_u) - \text{ROC}(u_0) \widehat{\mathcal{W}}_{\text{FPR}}(\hat{c}_u) + o_p(1) \end{aligned}$$

where $\text{ROC}(u_0) = \frac{\partial \text{ROC}(u_0)}{\partial u_0}$, $\widehat{\mathcal{W}}_{\text{TPR}}(c) = n^{1/2} \left[\widehat{\text{TPR}}_{\text{supROC}}(c) - \text{TPR}(c) \right]$, $\widehat{\mathcal{W}}_{\text{FPR}}(c) = n^{1/2} \left[\widehat{\text{FPR}}_{\text{supROC}}(c) - \text{FPR}(c) \right]$.

It therefore suffices to utilize the two steps outlined in Figure 1 to show that $\widehat{\mathcal{W}}_{\text{ROC}}(u_0)$ converges weakly to a zero-mean Gaussian distribution.

Key Steps

Step 1. Show that $\widehat{\mathcal{W}}_{\text{TPR}}(c)$ converges weakly to a zero mean Gaussian process.

Step 2. Show that $\widehat{\mathcal{W}}_{\text{FPR}}(c)$ converges weakly to a zero mean Gaussian process.

Figure 1: **Overview of the Proof**

Throughout we let g be a measurable function define $\mathbb{P}_n g = n^{-1} \sum_{i=1}^n g(X_i)$, $\mathbb{P}g = \int g dP$, and $\mathbb{G}_n g = n^{1/2}(\mathbb{P}_n g - \mathbb{P}g)$ be the scaled empirical process indexed by g .

Step 1: Weak convergence of $\widehat{\mathcal{W}}_{\text{TPR}}(c)$

We decompose $\widehat{\mathcal{W}}_{\text{TPR}}(c)$ into

$$\begin{aligned}\widehat{\mathcal{W}}_{\text{TPR}}(c) &= n^{1/2} \left[\widehat{\text{TPR}}_{\text{supROC}}(c; \widehat{\boldsymbol{\theta}}) - \text{TPR}(c; \widehat{\boldsymbol{\theta}}) \right] + n^{1/2} \left[\text{TPR}(c; \widehat{\boldsymbol{\theta}}) - \text{TPR}(c; \boldsymbol{\theta}^*) \right] \\ &= n^{1/2} \left[\widehat{\text{TPR}}_{\text{supROC}}(c; \widehat{\boldsymbol{\theta}}) - \text{TPR}(c; \widehat{\boldsymbol{\theta}}) \right] + n^{1/2} \nabla_{\boldsymbol{\theta}} \text{TPR}(c, \boldsymbol{\theta}^*) (\widehat{\boldsymbol{\theta}} - \boldsymbol{\theta}^*) + o_p(1)\end{aligned}\tag{1}$$

The second term of (1), which accounts for the variation in estimating $\boldsymbol{\theta}^*$, converges in probability to zero as $N^{1/2}(\widehat{\boldsymbol{\theta}} - \boldsymbol{\theta}^*) = O_p(1)$ and thus

$$n^{1/2} \nabla_{\boldsymbol{\theta}} \text{TPR}(c, \boldsymbol{\theta}^*) (\widehat{\boldsymbol{\theta}} - \boldsymbol{\theta}^*) = O_p[(n/N)^{1/2}] = o_p(1)$$

by Assumptions 1 and 2.

For the first term of (1), define $\widehat{\xi}(c, \boldsymbol{\theta}) = n^{-1} \sum_{i=1}^n I(S_{\boldsymbol{\theta}, i} \geq c) Y_i$, $\xi(c, \boldsymbol{\theta}) = \text{E}[I(S_{\boldsymbol{\theta}} \geq c) Y]$, and

$$\widehat{\mathcal{W}}_{\xi}(c, \boldsymbol{\theta}) = n^{1/2} \left[\widehat{\xi}(c, \boldsymbol{\theta}) - \xi(c, \boldsymbol{\theta}) \right] = \mathbb{G}_n[I(S_{\boldsymbol{\theta}} \geq c) Y].$$

Then,

$$\begin{aligned}n^{1/2} \left[\widehat{\text{TPR}}_{\text{supROC}}(c; \boldsymbol{\theta}) - \text{TPR}(c; \boldsymbol{\theta}) \right] &= n^{1/2} \left[\frac{\widehat{\xi}(c, \boldsymbol{\theta})}{\widehat{\xi}(0, \boldsymbol{\theta})} - \frac{\xi(c, \boldsymbol{\theta})}{\xi(0, \boldsymbol{\theta})} \right] \\ &= n^{1/2} \left\{ \frac{\widehat{\xi}(c, \boldsymbol{\theta}) - \xi(c, \boldsymbol{\theta})}{\widehat{\xi}(0, \boldsymbol{\theta})} + \xi(c, \boldsymbol{\theta}) \left[\frac{1}{\widehat{\xi}(0, \boldsymbol{\theta})} - \frac{1}{\xi(0, \boldsymbol{\theta})} \right] \right\} \\ &= \mu^{-1} \left[\widehat{\mathcal{W}}_{\xi}(c, \boldsymbol{\theta}) - \text{TPR}(c; \boldsymbol{\theta}) \widehat{\mathcal{W}}_{\xi}(0, \boldsymbol{\theta}) \right] \frac{\xi(0, \boldsymbol{\theta})}{\widehat{\xi}(0, \boldsymbol{\theta})},\end{aligned}$$

where $\mu = \text{E}(Y) = \xi(0, \boldsymbol{\theta})$.

By the uniform law of large numbers (ULLN) [Lemma 2.4, 9], $\sup_{\boldsymbol{\theta} \in \Theta} |\widehat{\xi}(c, \boldsymbol{\theta}) - \xi(c, \boldsymbol{\theta})| \xrightarrow{p} 0$

and $\xi(0, \boldsymbol{\theta})/\widehat{\xi}(0, \boldsymbol{\theta}) \xrightarrow{p} 1$. To establish the weak convergence of $\widehat{\mathcal{W}}_\xi(c, \boldsymbol{\theta})$, consider the class of functions

$$\{I(S_{\boldsymbol{\theta}} \geq c) : \boldsymbol{\theta} \in \Theta, c \in [0, 1]\}$$

which is a Vapnik-Chervonenkis class [Example 19.16, 10]. It follows that

$$\widehat{\mathcal{W}}_\xi(c, \boldsymbol{\theta}) = n^{-1/2} \sum_{i=1}^n [Y_i I(S_{\boldsymbol{\theta}, i} \geq c) - \mu \text{TPR}(c; \boldsymbol{\theta})]$$

converges weakly to a mean zero Gaussian process indexed by $(\boldsymbol{\theta}, c)$ and is stochastic equicontinuous in $(\boldsymbol{\theta}, c)$ so that

$$\begin{aligned} \widehat{\mathcal{W}}_{\text{TPR}}(c) &= \mu^{-1} \left[\widehat{\mathcal{W}}_\xi(c, \boldsymbol{\theta}^*) - \text{TPR}(c) \widehat{\mathcal{W}}_\xi(0, \boldsymbol{\theta}^*) \right] + o_p(1) \\ &= \mu^{-1} \left\{ n^{-1/2} \sum_{i=1}^n Y_i [I(S_i^* \geq c) - \text{TPR}(c)] \right\} + o_p(1) \\ &= n^{-1/2} \sum_{i=1}^n \mu^{-1} \{ (Y_i - \mu) [I(S_i^* \geq c) - \text{TPR}(c)] + \mu [I(S_i^* \geq c) - \text{TPR}(c)] \} + o_p(1). \end{aligned}$$

Step 2: Weak convergence of $\widehat{\mathcal{W}}_{\text{FPR}}(c)$

Let $\widehat{\zeta}(c, \boldsymbol{\theta}) = n^{-1} \sum_{i=1}^n I(S_{\boldsymbol{\theta}, i} \geq c)(1 - Y_i)$, $\zeta(c, \boldsymbol{\theta}) = \text{E}[I(S_{\boldsymbol{\theta}} \geq c)(1 - Y)]$, and

$$\widehat{\mathcal{W}}_\zeta(c, \boldsymbol{\theta}) = n^{1/2} \left[\widehat{\zeta}(c, \boldsymbol{\theta}) - \zeta(c, \boldsymbol{\theta}) \right] = \mathbb{G}_n[I(S_{\boldsymbol{\theta}} \geq c)(1 - Y)].$$

Using the same argument as in the previous section,

$$\widehat{\mathcal{W}}_{\text{FPR}}(c) = \mu_0^{-1} \left[\widehat{\mathcal{W}}_\zeta(c, \boldsymbol{\theta}) - \text{FPR}(c; \boldsymbol{\theta}) \widehat{\mathcal{W}}_\zeta(0, \boldsymbol{\theta}) \right] \frac{\zeta(0, \boldsymbol{\theta})}{\widehat{\zeta}(0, \boldsymbol{\theta})},$$

where $\mu_0 = 1 - \mu$. Using an analogous argument as the previous section,

$$\widehat{\mathcal{W}}_\zeta(c, \boldsymbol{\theta}) = n^{-1/2} \sum_{i=1}^n [(1 - Y_i) I(S_{\boldsymbol{\theta}, i} \geq c) - \mu_0 \text{FPR}(c; \boldsymbol{\theta})]$$

converges weakly to a mean zero Gaussian process indexed by $(\boldsymbol{\theta}, c)$, and is stochastic equicontinuous in $(\boldsymbol{\theta}, c)$ so that

$$\begin{aligned}\widehat{\mathcal{W}}_{\text{FPR}}(c) &= \mu_0^{-1} \left[\widehat{\mathcal{W}}_{\zeta}(c, \boldsymbol{\theta}^*) - \text{FPR}(c) \widehat{\mathcal{W}}_{\zeta}(0, \boldsymbol{\theta}^*) \right] + o_p(1) \\ &= \mu_0^{-1} \left\{ n^{-1/2} \sum_{i=1}^n (1 - Y_i) [I(S_i^* \geq c) - \text{FPR}(c)] \right\} + o_p(1) \\ &= n^{-1/2} \sum_{i=1}^n -\mu_0^{-1} \{ (Y_i - \mu) [I(S_i^* \geq c) - \text{FPR}(c)] - \mu_0^{-1} [I(S_i^* \geq c) - \text{FPR}(c)] \} + o_p(1).\end{aligned}$$

Using the fact that $\sup_{u_0 \in [0,1]} |\hat{c}_u - c_{u_0}| = o_p(1)$, it then follows that [Proposition 3.1–3.2, 11]

$$\begin{aligned}\widehat{\mathcal{W}}_{\text{ROC}}(u_0) &= \widehat{\mathcal{W}}_{\text{TPR}}(c_{u_0}) - \text{ROC}(u_0) \widehat{\mathcal{W}}_{\text{FPR}}(c_{u_0}) + o_p(1) \\ &= n^{-1/2} \sum_{i=1}^n [\mathcal{G}_i(S; \boldsymbol{\theta}^*, c_{u_0})(Y_i - \mu) + \Gamma_i(S; \boldsymbol{\theta}^*, c_{u_0})] + o_p(1) \\ &= n^{-1/2} \sum_{i=1}^n IF_{\text{supROC}}(Y_i, S_i; \boldsymbol{\theta}^*, c_{u_0}) + o_p(1)\end{aligned}$$

where $\mathcal{G}_i(S; \boldsymbol{\theta}^*, c_{u_0}) = \left[\mu^{-1} + \mu_0^{-1} \text{ROC}(u_0) \right] I(S_i^* \geq c_{u_0}) - \left[\mu^{-1} \text{ROC}(u_0) + \mu_0^{-1} \text{ROC}(u_0) u_0 \right]$, $\Gamma_i(S; \boldsymbol{\theta}^*, c_{u_0}) = I(S_i^* \geq c_{u_0}) - \text{ROC}(u_0) - \text{ROC}(u_0) [I(S_i^* \geq c_{u_0}) - u_0]$, and $IF_{\text{supROC}}(Y_i, S_i; \boldsymbol{\theta}^*, c_{u_0}) = \mathcal{G}_i(S; \boldsymbol{\theta}^*, c_{u_0})(Y_i - \mu) + \Gamma_i(S; \boldsymbol{\theta}^*, c_{u_0})$. Therefore, $\widehat{\mathcal{W}}_{\text{ROC}}(u_0)$ is asymptotically Gaussian with mean zero and variance $E\{[IF_{\text{supROC}}(Y, S; \boldsymbol{\theta}^*, c_{u_0})]^2\}$.

2.2 Semi-supervised Estimator

We follow the same general steps as in Figure 1 to study the weak convergence of the semi-supervised estimator.

Similar as before, we let g be a measurable function define $\mathbb{P}_N g = N^{-1} \sum_{i=n+1}^{n+N} g(X_i)$, and $\mathbb{G}_N g = N^{1/2}(\mathbb{P}_N g - \mathbb{P}g)$ be the scaled empirical process indexed by g .

Step 1: Weak convergence of $\widetilde{\mathcal{W}}_{\text{TPR}}(c)$

Let $\tilde{\xi}(c, \boldsymbol{\theta}) = N^{-1} \sum_{i=n+1}^{n+N} I(S_{\boldsymbol{\theta},i} \geq c) \widehat{m}(S_{\boldsymbol{\theta},i})$ and $\xi(c, \boldsymbol{\theta}) = \mathbb{E}[I(S_{\boldsymbol{\theta}} \geq c)Y] = \mathbb{E}[I(S_{\boldsymbol{\theta}} \geq c)m(S_{\boldsymbol{\theta}})]$. Following the same steps as in Figure 1, we establish the weak convergence of

$$\begin{aligned} \widetilde{\mathcal{W}}_{\xi}(c, \boldsymbol{\theta}) &= n^{1/2} \left[\tilde{\xi}(c, \boldsymbol{\theta}) - \xi(c, \boldsymbol{\theta}) \right] \\ &= \widetilde{\mathcal{W}}_{\xi,a} + \widetilde{\mathcal{W}}_{\xi,b}, \end{aligned}$$

where $\widetilde{\mathcal{W}}_{\xi,a} = n^{1/2} \mathbb{P}_N \{I(S_{\boldsymbol{\theta}} \geq c) [\widehat{m}(S_{\boldsymbol{\theta}}) - m(S_{\boldsymbol{\theta}})]\}$ and $\widetilde{\mathcal{W}}_{\xi,b} = (n/N)^{1/2} \mathbb{G}_N [I(S_{\boldsymbol{\theta}} \geq c)m(S_{\boldsymbol{\theta}})]$.

For $\widetilde{\mathcal{W}}_{\xi,b}$, we note that $\mathbb{G}_N [I(S_{\boldsymbol{\theta}} \geq c)m(S_{\boldsymbol{\theta}})]$ converges weakly to a Gaussian process by the functional Central Limit Theorem [Theorem 10.6, 12] and therefore

$$\widetilde{\mathcal{W}}_{\xi,b} = (n/N)^{1/2} \mathbb{G}_N [I(S_{\boldsymbol{\theta}} \geq c)m(S_{\boldsymbol{\theta}})] = O_p \left[(n/N)^{1/2} \right] = o_p(1).$$

For $\widetilde{\mathcal{W}}_{\xi,a}$, we write $\widetilde{\mathcal{W}}_{\xi,a} = \widetilde{\mathcal{W}}_{\xi,a_1} + \widetilde{\mathcal{W}}_{\xi,a_2}$, where

$$\begin{aligned} \widetilde{\mathcal{W}}_{\xi,a_1} &= n^{1/2} (\mathbb{P}_N - \mathbb{P}) \{I(S_{\boldsymbol{\theta}} \geq c) [\widehat{m}(S_{\boldsymbol{\theta}}) - m(S_{\boldsymbol{\theta}})]\} \\ \widetilde{\mathcal{W}}_{\xi,a_2} &= n^{1/2} \mathbb{P} \{I(S_{\boldsymbol{\theta}} \geq c) [\widehat{m}(S_{\boldsymbol{\theta}}) - m(S_{\boldsymbol{\theta}})]\}. \end{aligned}$$

We first evaluate $\widetilde{\mathcal{W}}_{\xi,a_1}$ by considering $\epsilon_i = \{I(S_{\boldsymbol{\theta},i} \geq c) [\widehat{m}(S_{\boldsymbol{\theta},i}) - m(S_{\boldsymbol{\theta},i})]\}_{i=n+1, \dots, n+N}$. Note that ϵ_i are independent conditional on the labeled data and bounded by $|\epsilon_i| \leq \sup_{\mathbf{Z}} |\widehat{m}[S(\mathbf{Z}; \boldsymbol{\theta})] - m[S(\mathbf{Z}; \boldsymbol{\theta})]| = o_p(1) \leq M$ almost surely, for some constant $M < \infty$. Applying Hoeffding's inequality conditional on the labeled data, we have for any $t > 0$,

$$P \left(\sum_{i=1}^N [\epsilon_i - \mathbb{E}(\epsilon_i)] \geq N^{1/2} t \right) \leq \exp \left(-\frac{2Nt^2}{NM^2} \right).$$

Hence $\widetilde{\mathcal{W}}_{\xi,a_1} = O_p \left[(n/N)^{1/2} \right] = o_p(1)$.

Next, to evaluate $\widetilde{\mathcal{W}}_{\xi, a_2}$ we further decompose the term as

$$\begin{aligned}
\widetilde{\mathcal{W}}_{\xi, a_2} &= n^{1/2} \int_c^1 [\widehat{m}(s_{\boldsymbol{\theta}}) - m(s_{\boldsymbol{\theta}})] f(s_{\boldsymbol{\theta}}) ds_{\boldsymbol{\theta}} \\
&= n^{1/2} \int_c^1 [\widehat{m}(s_{\boldsymbol{\theta}}) - m(s_{\boldsymbol{\theta}})] \left[f(s_{\boldsymbol{\theta}}) + \widehat{f}(s_{\boldsymbol{\theta}}) - \widehat{f}(s_{\boldsymbol{\theta}}) \right] ds_{\boldsymbol{\theta}} \\
&= n^{1/2} \int_c^1 \sum_{i=1}^n \frac{1}{nh} K_h(S_{\boldsymbol{\theta}, i} - s_{\boldsymbol{\theta}}) [Y_i - m(s_{\boldsymbol{\theta}})] ds_{\boldsymbol{\theta}} + n^{1/2} \int_c^1 [\widehat{m}(s_{\boldsymbol{\theta}}) - m(s_{\boldsymbol{\theta}})] \left[f(s_{\boldsymbol{\theta}}) - \widehat{f}(s_{\boldsymbol{\theta}}) \right] ds_{\boldsymbol{\theta}} \\
&= \widetilde{\mathcal{W}}_{\xi, a_{21}} + \widetilde{\mathcal{W}}_{\xi, a_{22}},
\end{aligned}$$

where $\widehat{f}(s) = \frac{1}{n} \sum_{i=1}^n K_h(S_{\boldsymbol{\theta}, i} - s_{\boldsymbol{\theta}})$.

From Assumption 3, it follows from [Lemma 1 and Theorem B, 13] that

$$\widetilde{\mathcal{W}}_{\xi, a_{22}} \leq n^{1/2} \sup_{s_{\boldsymbol{\theta}} \in [c, 1]} |\widehat{m}(s_{\boldsymbol{\theta}}) - m(s_{\boldsymbol{\theta}})| \sup_{s_{\boldsymbol{\theta}} \in [c, 1]} |f(s_{\boldsymbol{\theta}}) - \widehat{f}(s_{\boldsymbol{\theta}})| = O_p \left[\frac{\log(1/h)}{n^{1/2}h} \right] = o_p(1).$$

For $\widetilde{\mathcal{W}}_{\xi, a_{21}}$, we substitute $u_0 = (s_{\boldsymbol{\theta}} - S_{\boldsymbol{\theta}, i})/h$ and apply Taylor's expansion at $S_{\boldsymbol{\theta}, i}$,

$$\begin{aligned}
\widetilde{\mathcal{W}}_{\xi, a_{21}} &= n^{-1/2} \sum_{i=1}^n \int_{(c-S_{\boldsymbol{\theta}, i})/h}^{(1-S_{\boldsymbol{\theta}, i})/h} K(u_0) [Y_i - m(hu_0 + S_{\boldsymbol{\theta}, i})] du \\
&= n^{-1/2} \sum_{i=1}^n \int_{(c-1)/h}^{(1-c)/h} I(S_{\boldsymbol{\theta}, i} \geq c) K(u_0) [Y_i - m(S_{\boldsymbol{\theta}, i}) - uhm'(S_{\boldsymbol{\theta}, i}) - u_0^2 h^2 m''(S_{\boldsymbol{\theta}, i})/2 + o(h^2)] du \\
&= n^{-1/2} \sum_{i=1}^n I(S_{\boldsymbol{\theta}, i} \geq c) [Y_i - m(S_{\boldsymbol{\theta}, i})] + O_p(n^{1/2}h^2)
\end{aligned}$$

It then follows that

$$\widetilde{\mathcal{W}}_{\xi}(c, \boldsymbol{\theta}) = n^{-1/2} \sum_{i=1}^n I(S_{\boldsymbol{\theta}, i} \geq c) [Y_i - m(S_{\boldsymbol{\theta}, i})] + o_p(1)$$

converges weakly to a mean zero Gaussian process indexed by $(\boldsymbol{\theta}, c)$, by the functional Central Limit Theorem [Theorem 10.6, 12] and is stochastic equicontinuous in $(\boldsymbol{\theta}, c)$.

Thus,

$$\begin{aligned}\widetilde{\mathcal{W}}_{\text{TPR}}(c) &= \mu^{-1} \left[\widetilde{\mathcal{W}}_{\xi}(c, \boldsymbol{\theta}^*) - \text{TPR}(c) \widetilde{\mathcal{W}}_{\xi}(0, \boldsymbol{\theta}^*) \right] + o_p(1) \\ &= n^{-1/2} \sum_{i=1}^n \mu^{-1} \{ [Y_i - m(S_i^*)] [I(S_i^* \geq c) - \text{TPR}(c)] \} + o_p(1).\end{aligned}$$

Step 2: Weak convergence of $\widetilde{\mathcal{W}}_{\text{FPR}}(c)$

Let $\tilde{\zeta}(c, \boldsymbol{\theta}) = N^{-1} \sum_{i=n+1}^{n+N} I(S_{\boldsymbol{\theta},i} \geq c) [1 - \widehat{m}(S_{\boldsymbol{\theta},i})]$, $\zeta(c, \boldsymbol{\theta}) = \text{E} \{ I(S_{\boldsymbol{\theta}} \geq c) [1 - m(S_{\boldsymbol{\theta}})] \}$, and

$$\widetilde{\mathcal{W}}_{\zeta}(c, \boldsymbol{\theta}) = n^{1/2} \left[\tilde{\zeta}(c, \boldsymbol{\theta}) - \zeta(c, \boldsymbol{\theta}) \right].$$

Using the same argument as in the previous section,

$$\widetilde{\mathcal{W}}_{\text{FPR}}(c) = \mu_0^{-1} \left[\widetilde{\mathcal{W}}_{\zeta}(c, \boldsymbol{\theta}) - \text{FPR}(c; \boldsymbol{\theta}) \widetilde{\mathcal{W}}_{\zeta}(0, \boldsymbol{\theta}) \right] \frac{\zeta(0, \boldsymbol{\theta})}{\zeta(0, \boldsymbol{\theta})},$$

where $\mu_0 = 1 - \mu$. Using analogous arguments as the supervised setting,

$$\widetilde{\mathcal{W}}_{\zeta}(c, \boldsymbol{\theta}) = n^{-1/2} \sum_{i=1}^n \{ [m(S_{\boldsymbol{\theta},i}) - Y_i] I(S_{\boldsymbol{\theta},i} \geq c) \}$$

converges weakly to a mean zero Gaussian process index by $(\boldsymbol{\theta}, c)$, and is stochastic equicontinuous in $(\boldsymbol{\theta}, c)$ so that

$$\begin{aligned}\widetilde{\mathcal{W}}_{\text{FPR}}(c) &= \mu_0^{-1} \left[\widetilde{\mathcal{W}}_{\xi}(c, \boldsymbol{\theta}^*) - \text{FPR}(c) \widetilde{\mathcal{W}}_{\xi}(0, \boldsymbol{\theta}^*) \right] + o_p(1) \\ &= n^{-1/2} \sum_{i=1}^n -\mu_0^{-1} \{ [Y_i - m(S_i^*)] [I(S_i^* \geq c) - \text{FPR}(c)] \} + o_p(1).\end{aligned}$$

It then follows that

$$\begin{aligned}
\widetilde{\mathcal{W}}_{\text{ROC}}(u_0) &= \widetilde{\mathcal{W}}_{\text{TPR}}(c_{u_0}) - \text{ROC}(u_0)\widetilde{\mathcal{W}}_{\text{FPR}}(c_{u_0}) + o_p(1) \\
&= n^{-1/2} \sum_{i=1}^n \mathcal{G}_i(S; \boldsymbol{\theta}^*, c_{u_0}) [Y_i - m(S_i^*)] + o_p(1) \\
&= n^{-1/2} \sum_{i=1}^n IF_{ss\text{ROC}}(Y_i; \boldsymbol{\theta}^*, c_{u_0}) + o_p(1)
\end{aligned}$$

where $\mathcal{G}_i(S; \boldsymbol{\theta}^*, c_{u_0}) = \left[\mu^{-1} + \mu_0^{-1} \text{ROC}(u_0) \right] I(S_i^* \geq c_{u_0}) - \left[\mu^{-1} \text{ROC}(u_0) + \mu_0^{-1} \text{ROC}(u_0) u_0 \right]$, and $IF_{ss\text{ROC}}(Y_i, S_i; \boldsymbol{\theta}^*, c_{u_0}) = \mathcal{G}_i(S; \boldsymbol{\theta}^*, c_{u_0}) [Y_i - m(S_i^*)]$. Therefore, $\widetilde{\mathcal{W}}_{\text{ROC}}(u_0)$ is asymptotically Gaussian with mean zero and variance $E\{[IF_{ss\text{ROC}}(Y, S; \boldsymbol{\theta}^*, c_{u_0})]^2\}$.

3 Description of the PheNorm Algorithm

We briefly outline the PheNorm algorithm proposed by [4], which consists of three key steps. We do not use the random corruption denoising step as it showed limited improvement in the original paper.

Step I: Raw Feature Extraction. The input data for PheNorm is patient-level data on $(x_{ICD}, x_{NLP}, x_{ICDNLP}, x_{HU})$. The *silver-standard labels* are x_{ICD} , x_{NLP} , and $x_{ICDNLP} = x_{ICD} + x_{NLP}$. x_{ICD} and x_{NLP} are the counts of phenotype-specific ICD codes and free-text positive mentions of target phenotype in a patient’s record. x_{ICDNLP} is a derived feature that can be more predictive of the underlying phenotype than x_{ICD} or x_{NLP} alone. x_{HU} is a feature measuring *healthcare utilization* such as the count of the total number of notes in a patient’s record or the number of encounters in the billing system.

Step II: Normal Mixture Normalization. The silver-standard labels are normalized against x_{HU} to account for the fact that patients with higher healthcare utilization tend to have more ICD codes and free-text positive mentions of target phenotype, irrespective of their true disease status. The key idea of PheNorm is that the normalized silver standard labels approximately follow a normal mixture model.

Specifically, let

$$z = \log(1 + x_s) - \alpha \log(1 + x_{HU})$$

be a normalized silver-standard label for some $\alpha \in (0, 1)$ and $s \in (ICD, NLP, ICDNLP)$.

PheNorms assumes

$$z \sim \mu N(\tau_1, \sigma^2) + (1 - \mu)N(\tau_0, \sigma^2)$$

where $\mu = P(Y = 1)$, τ_1 and τ_0 are the means corresponding to the phenotype case and control groups, respectively, and σ^2 is a common variance parameter. The PheNorm

algorithm finds estimates for $(\alpha, \mu, \tau_0, \tau_1, \sigma)$ through the expectation-maximization (EM) algorithm. The optimal value of the normalization coefficient, α , minimizes the distribution divergence between the empirical distribution of the observed z and the normal mixture approximation. For a given α , the EM algorithm is used to find the maximum likelihood estimates of $(\mu, \tau_0, \tau_1, \sigma)$, and the distributional divergence is calculated using the parameter estimates.

Step III: Majority Voting. The normal mixture approximation in Step II is utilized for all three of the silver-standard labels. With the normal mixture parameter estimates, the posterior probability of the phenotype is calculated based on each silver standard label. The final PheNorm score is the average of the three posterior probabilities.

4 Simulation Study

Metric	n	Method	ESE	ASE	Coverage Probability	
					Standard Wald	Logit-based
AUC	100	supROC	5.50	5.41	93.75	95.40
		ssROC	5.42	4.97	91.70	93.10
	200	supROC	3.74	3.77	94.70	95.90
		ssROC	3.64	3.52	93.70	94.35
Threshold	100	supROC	5.93	6.06	92.35	93.20
		ssROC	5.51	4.93	89.45	90.60
	200	supROC	4.30	4.51	94.00	94.15
		ssROC	3.77	3.75	91.20	91.60
TPR	100	supROC	9.31	9.18	93.70	95.60
		ssROC	9.14	8.13	90.15	91.85
	200	supROC	6.59	6.91	94.50	95.60
		ssROC	6.23	6.19	91.55	92.35
PPV	100	supROC	4.83	4.83	94.90	95.65
		ssROC	4.61	3.97	92.25	92.45
	200	supROC	3.16	3.44	95.75	95.70
		ssROC	2.84	2.97	93.90	94.55
NPV	100	supROC	6.41	6.30	94.45	95.35
		ssROC	6.46	6.05	93.15	94.50
	200	supROC	4.47	4.56	95.30	96.15
		ssROC	4.43	4.38	94.65	95.35

Table 1: **Coverage Probability for simulation setting 1 at a FPR of 10%.** Coverage Probability (CP) of the 95% confidence intervals for the ROC parameters with labeled data sizes $n = 100$ and 200 for simulation setting 1 (PA with low accuracy). The size of the unlabeled data was $N = 10,000$. ESE: Empirical Standard Error; ASE: Asymptotic Standard Error.

Metric	n	Method	ESE	ASE	Coverage Probability	
					Standard Wald	Logit-based
AUC	100	supROC	1.98	1.93	90.10	96.90
		ssROC	1.76	1.58	89.50	93.50
	200	supROC	1.37	1.35	92.70	96.00
		ssROC	1.20	1.15	91.50	94.35
Threshold	100	supROC	4.24	4.45	92.95	93.25
		ssROC	3.25	3.19	92.20	92.35
	200	supROC	3.09	3.12	92.40	92.40
		ssROC	2.38	2.29	92.45	92.70
TPR	100	supROC	7.64	7.96	93.70	97.65
		ssROC	6.39	6.33	92.10	96.25
	200	supROC	5.52	5.63	93.30	97.85
		ssROC	4.62	4.58	92.95	96.40
PPV	100	supROC	3.21	3.32	95.65	95.85
		ssROC	2.00	2.04	93.50	93.35
	200	supROC	2.19	2.25	95.60	95.70
		ssROC	1.44	1.41	93.90	94.15
NPV	100	supROC	4.61	4.74	93.05	97.20
		ssROC	3.76	3.67	92.10	96.85
	200	supROC	3.30	3.37	93.35	97.85
		ssROC	2.68	2.67	93.50	96.05

Table 2: **Coverage Probability for simulation setting 2 at a FPR of 10%.** Coverage Probability (CP) of the 95% confidence intervals for the ROC parameters with labeled data sizes $n = 100$ and 200 for simulation setting 2 (PA with high accuracy). The size of the unlabeled data was $N = 10,000$. ESE: Empirical Standard Error; ASE: Asymptotic Standard Error.

5 Analysis of Eight PAs from MGB

5.1 Confidence Intervals

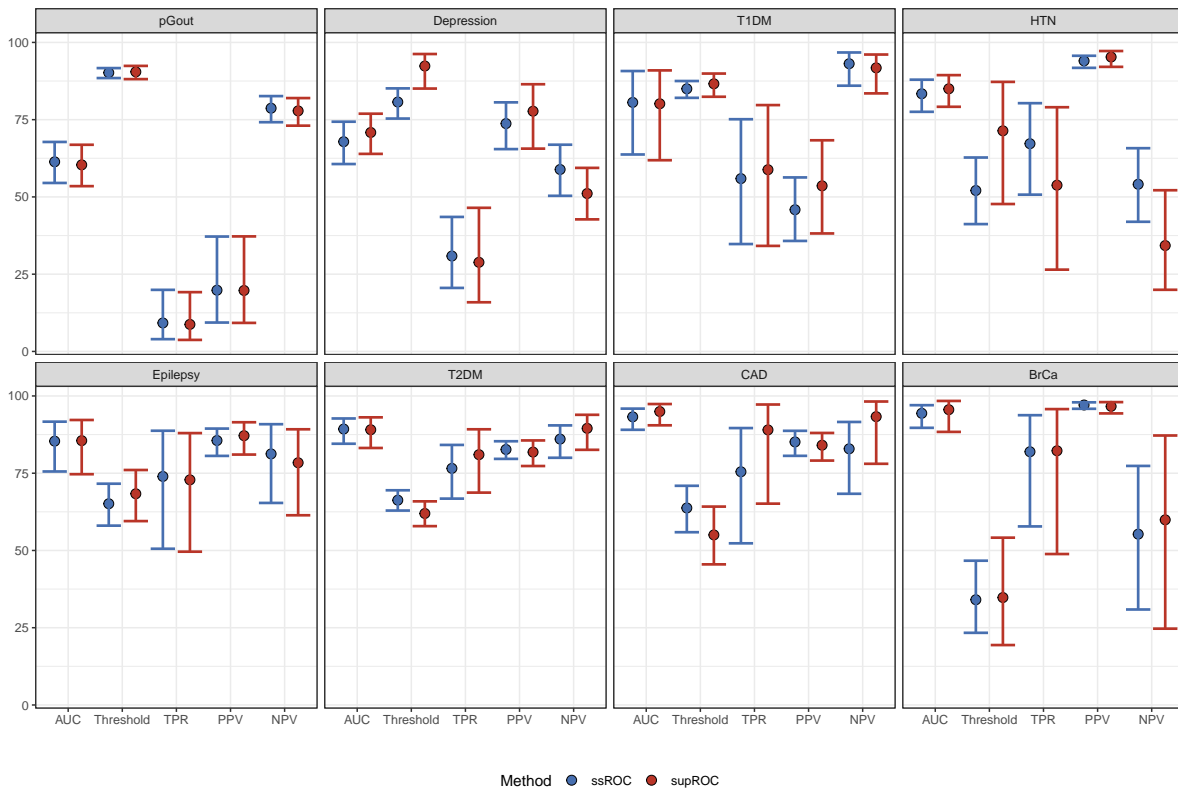


Figure 2: **95% confidence intervals at a FPR of 10%**. Point estimates and the 95% logit-based confidence intervals of the ROC parameter estimates for both ssROC and supROC for the 8 MGB phenotypes.

5.2 Relative Efficiency

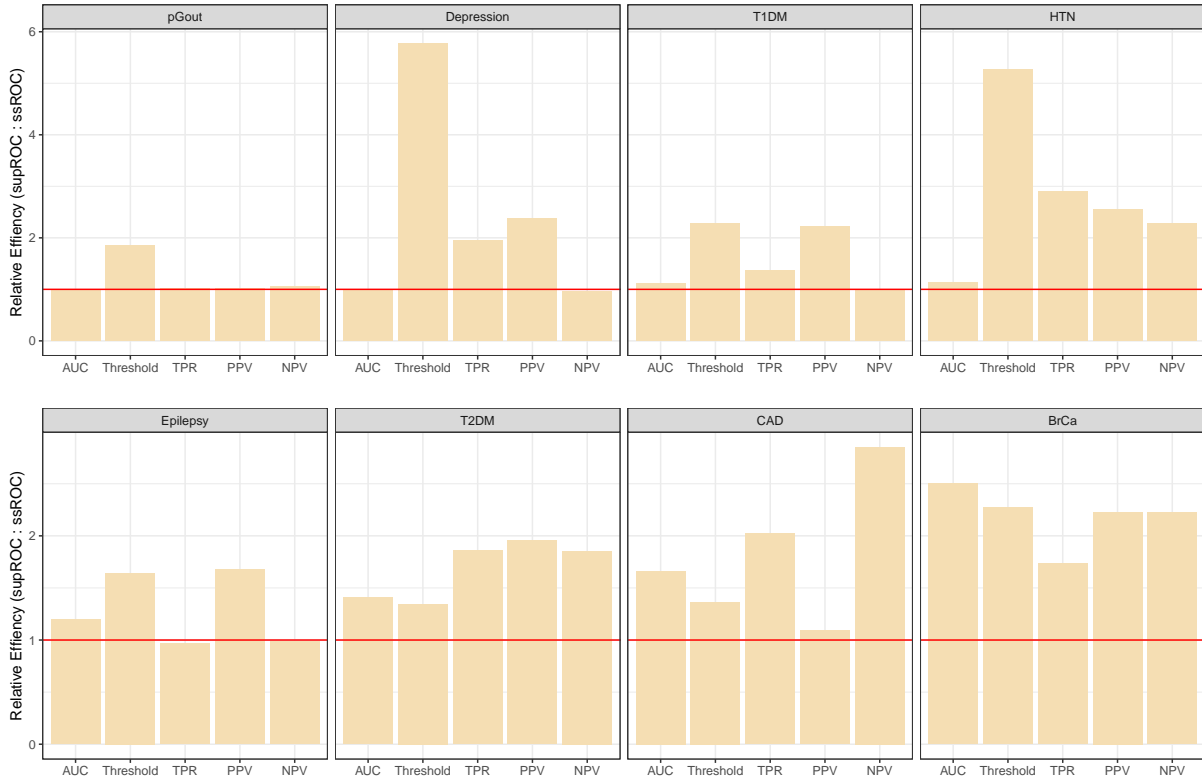


Figure 3: **Relative efficiency at a FPR of 10%.** The relative efficiency (RE) of supROC versus ssROC for the ROC parameters for the 8 MGB phenotypes. RE is defined as the ratio of the variance of supROC to that of ssROC.

5.3 Perturbation Resampling

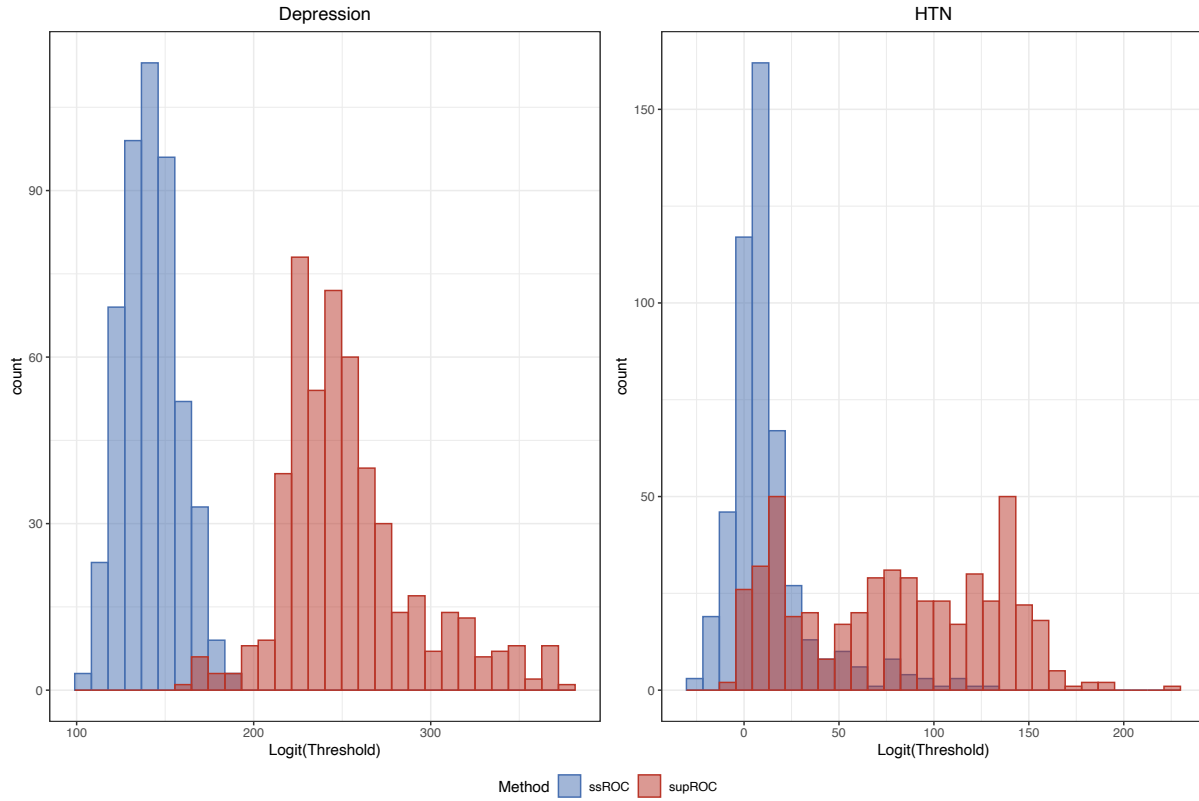


Figure 4: **Empirical Distribution of the Perturbed Threshold at a FPR of 10%.** Distribution of the logit-transformed classification threshold estimates from 500 replicates of the perturbation resampling procedure for Depression and Hypertension (HTN).

References

1. Jin, Z., Ying, Z. & Wei, L. A Simple Resampling Method by Perturbing the Minimax. *Biometrika* **88**, 381–390 (June 2001).
2. Gronsbell, J. L. & Cai, T. Semi-supervised approaches to efficient evaluation of model prediction performance. *Journal of the Royal Statistical Society: Series B (Statistical Methodology)* **80**, 579–594 (2018).
3. Agresti, A. *Categorical data analysis* (John Wiley & Sons, 2012).
4. Yu, S., Ma, Y., Gronsbell, J., *et al.* Enabling phenotypic big data with PheNorm. *Journal of the American Medical Informatics Association* **25**, 54–60 (2018).
5. Gronsbell, J., Minnier, J., Yu, S., *et al.* Automated feature selection of predictors in electronic medical records data. *Biometrics* **75**, 268–277 (2019).
6. Agarwal, V., Podchiyska, T., Banda, J. M., *et al.* Learning statistical models of phenotypes using noisy labeled training data. *Journal of the American Medical Informatics Association* **23**, 1166–1173 (2016).
7. Banda, J. M., Halpern, Y., Sontag, D., *et al.* Electronic phenotyping with APHRODITE and the Observational Health Sciences and Informatics (OHDSI) data network. *AMIA Summits on Translational Science Proceedings* **2017**, 48–57 (July 2017).
8. Van der Vaart, A. W. *Asymptotic statistics* (Cambridge University Press, 2000).
9. Newey, W. K. & McFadden, D. in *Handbook of Econometrics* 2111–2245 (Elsevier, Jan. 1994).
10. Van der Vaart, A. W. *Asymptotic Statistics* (Cambridge University Press, Cambridge, UK ; New York, NY, USA, 1998).
11. Bogoya, J. M., Böttcher, A. & Maximenko, E. A. From Convergence in Distribution to Uniform Convergence. *Boletín de la Sociedad Matemática Mexicana* **22**, 695–710 (Oct. 2016).

12. Pollard, D. *Empirical processes: theory and applications* in *NSF-CBMS regional conference series in probability and statistics* (1990), i–86.
13. Mack, Y. P. & Silverman, B. W. Weak and Strong Uniform Consistency of Kernel Regression Estimates. *Zeitschrift für Wahrscheinlichkeitstheorie und Verwandte Gebiete* **61**, 405–415 (Sept. 1982).